

# Fluxon Time-Delay Readout of a Superconducting Qubit Protected by a Spectral Gap in a Josephson Transmission Line

Shunsuke Kamimura,<sup>1,2,\*</sup> Aree Taguchi,<sup>2,3</sup> Masamitsu Tanaka,<sup>4</sup> and Tsuyoshi Yamamoto<sup>1,3,5,†</sup>

<sup>1</sup>*Secure System Platform Research Laboratories,  
NEC Corporation, Kawasaki, Kanagawa, Japan*

<sup>2</sup>*NEC-AIST Quantum Technology Cooperative Research Laboratory, Tsukuba, Ibaraki 305-8568, Japan*

<sup>3</sup>*Division of Physics, Faculty of Pure and Applied Sciences,  
University of Tsukuba, Tennodai, Tsukuba, Ibaraki 305-8571, Japan*

<sup>4</sup>*Graduate School of Engineering, Nagoya University, Nagoya, Aichi 464-8603, Japan*

<sup>5</sup>*Global Research and Development Center for Business by Quantum-AI technology (G-QuAT),  
National Institute of Advanced Industrial Science and Technology (AIST), Tsukuba, Ibaraki, Japan*

We theoretically investigate a readout scheme of the quantum state of a superconducting qubit based on time delay of a single flux quantum (SFQ), also known as a fluxon, propagating in a Josephson transmission line (JTL). We concretely study the time-delay readout based on capacitive coupling between a transmon qubit and a JTL, and we evaluate the time delay depending on the qubit state. We also reveal a feature of the absence of fluxon pinning and exponential suppression of nonadiabatic transitions caused by the propagating fluxon, which is advantageous for the time-delay readout. We extend the analysis to a multi-level transmon as well. Owing to the spectral gap in the JTL, the radiative decay of the qubit mediated by the JTL is exponentially suppressed, and thus the transmission line itself also serves as a filter protecting the qubit. The readout scheme requires neither complicated wiring to low-temperature stages nor bulky microwave components, which are bottlenecks for integration of a large-scale superconducting quantum computer.

## I. INTRODUCTION

Superconducting quantum circuits are leading candidates for a scalable quantum computer since the first realization of a single superconducting qubit [1], and its various modifications have been invented [2–6]. However, the hardware overhead is immense to demonstrate computational advantage [7–9] of a large-scale fault tolerant quantum computer [10–13], due to required wiring to qubits and thermal-load overheads under the brute-force scaling with current technology [14]. Especially for qubit readout, which is one of the criteria for a scalable quantum computer [15], today’s systems largely rely on a near quantum-limited amplifier, bulky microwave components such as circulators, an amplifier based on high-electron-mobility transistor (HEMT), and subsequent heterodyne detection and thresholding at room temperature [16], which inevitably involves the significant overheads.

When reading out the quantum state of a superconducting qubit, we often confront a trade-off that strong coupling to an external apparatus to accurately infer the quantum state inevitably induces noise for the qubit. For the most standard readout scheme referred to as the dispersive readout [17–19], a strong coupling between the qubit and a readout resonator induces a large frequency shift of the resonator depending on the qubit state, while much strong coupling also gives rise to fast radiative decay of qubit into an environment, which significantly destroys the qubit coherence [17, 20–24]. To

suppress the radiative decay into the environment, one can utilize a filter, referred to as a Purcell filter [25–27], that reduces the resonator density of states at the qubit frequency [28]. In addition to such radiative decay, unwanted state transitions caused by microwave readout drive inside or outside the qubit subspace, or related state leakage referred to as qubit ionizations, are being actively investigated [29–38].

Towards realization of a large-scale superconducting quantum computer, one feasible approach is heterogeneous quantum-classical architecture relying on the use of superconducting single-flux-quantum (SFQ) based digital logic, such as rapid single flux quantum (RSFQ) [39], energy-efficient RSFQ (ERSFQ) [40], and ultra low-power, adiabatic quantum flux parametron (AQFP) [41] to mitigate the wiring and thermal-load overheads [14, 42–45]. On the one hand, for a qubit control based on SFQ circuits, theoretical proposals for single-qubit and two-qubit gates are presented [46–50], and a single-qubit gate has already been experimentally demonstrated [51–53]. On the other hand, in spite of theoretical [54–59] and related experimental results [60–65], the experimental demonstration of a qubit readout scheme within a low-temperature stage remains elusive.

We investigate a readout scheme based on time delay of a SFQ, also called a fluxon, caused by a superconducting qubit. The time-delay readout scheme has been proposed [54] and theoretically studied in detail [55] for inductive coupling between a flux qubit and a nonlinear transmission line hosting a propagating fluxon, which is called a Josephson transmission line (JTL). We consider the time-delay readout of a transmon qubit [4] capacitively coupled to a JTL and find analytical and numerical results of time delay based on the perturbation theory of the JTL [66, 67]. We reveal a distinct feature

---

\* shunsuke1997213@gmail.com

† tsuyoshi.yamamoto@aist.go.jp

regarding the pinning effect of fluxon for capacitive coupling to a transmon qubit; a fluxon is not pinned by the capacitive coupling even for an arbitrarily slow fluxon, while there is a finite pinning velocity for the inductive coupling below which the fluxon is pinned by an effective potential [55, 68]. This feature of the capacitive coupling is advantageous over the inductive coupling, in that one can obtain a large amount of time delay by slowing the initial velocity of the fluxon without suffering from the pinning effect. Also, as is done in the previous study [55], we estimate the degree of nonadiabatic transitions caused by the capacitive coupling to the JTL and find exponentially suppressed transition probabilities with respect to the fluxon velocity. We also consider a multi-level transmon and derive analytical results of time delay depending on the photon-number states of the transmon, and we discuss the absence of fluxon pinning and unwanted state transitions inside and outside the qubit subspace.

Furthermore, we study radiative decay of a transmon qubit mediated by a JTL. Based on the observation that only small-amplitude oscillations are relevant to typical low-impedance JTLs possessing no fluxon [69], we approximate a JTL by a “linearized” but massive transmission line that we call a Klein–Gordon transmission line (KGTL) after the equation of motion it obeys. By calculating the admittance of a dissipationless KGTL seen by a capacitively coupled transmon, we find an exponential suppression of the radiative decay rate due to an external source. This originates from a spectral gap appearing in the KGTL’s dispersion relation rooted in the mass term of the Klein–Gordon equation. Thus, the JTL serves not only as a medium transmitting the fluxon but also as a filter protecting the qubit from the environment. In typical circumstances, even though we have a finite amount of the qubit decay rate caused by a so-called subgap resistance responsible for a leakage current of the JTL, the amount of induced dissipation is relatively small for typical underdamped JTLs, and we can ignore its impact on the qubit coherence.

The remainder of this paper is organized as follows. In Sec. II, we provide classical Hamiltonians of the total system composed of a transmon, a JTL, and a coupling capacitor in between, and the perturbation theory of JTL is briefly reviewed in this section. Also, we address the quantum-mechanical treatment of the transmon and typical values of circuit parameters. In Sec. III, we give analytical and numerical results of the time delay induced by capacitive coupling with a transmon qubit under the two-level approximation. In this section, we discuss the absence of pinning and nonadiabatic unwanted state transitions, and a method to enhance the readout precision via bias current is theoretically and numerically examined. We also presents typical time resolutions of delay detection based on SFQ digital circuits. In Sec. IV, we extend the discussion to a multi-level transmon. In Sec. V, the degree of radiative decay is calculated for a dissipationless JTL based on the approximation by a KGTL, and also the decay

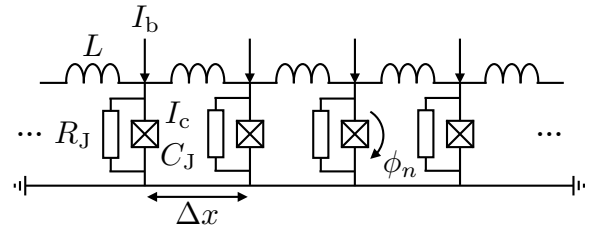


FIG. 1. Schematic diagram of a discrete JTL, also called a lumped-element JTL, which is made of JJs connected each other via linear inductors. Each cell of length  $\Delta x$  is characterized by the junction capacitance  $C_J$ , the junction critical current  $I_c$ , and the inductance  $L$  of the upper electrode. Each junction is subject to a bias current  $I_b$ , and a resistor  $R_J = 1/G_J$  describes normal current flowing across the junction. The discrete JTL gives a circuit model of a continuous JTL, which is also known as a long Josephson junction (LJJ).

rate for a dissipative but underdamped JTL is evaluated to incorporate more practical circumstances. Finally, in Sec. VI, we provide discussions and perspectives of the present study, and a conclusion follows in Sec. VII.

## II. MODEL

### A. Josephson transmission line (JTL) and sine-Gordon equation

A discrete JTL is made of Josephson junctions (JJs) connected each other via linear inductors of an inductance  $L$  (See Fig. 1). The JTL also has the capacitance  $C_J$  and the Josephson energy  $E_J$  of JJs per unit cell of length  $\Delta x$ , the latter of which is related to the junction critical current  $I_c$ , as  $E_J := \varphi_0 I_c$ . Here,  $\varphi_0 := \hbar/(2e) \simeq 3.29 \times 10^{-16}$  Wb denotes the reduced magnetic flux quantum, which is defined by the reduced Planck constant  $\hbar = h/(2\pi)$  and the elementary charge  $e$ . From Kirchhoff’s current and voltage laws, we construct a classical Hamiltonian  $H_{\text{JTL}}$  of the JTL, as

$$H_{\text{JTL}} = \sum_{n=0}^N \left[ \frac{Q_n^2}{2C_J} + \frac{\varphi_0^2}{2L} (\phi_{n+1} - \phi_n)^2 - E_J \cos \phi_n \right], \quad (1)$$

where the physical variables of the  $n$ -th junction are the conjugate charge  $Q_n$  to the flux  $\Phi_n$  and the dimensionless phase  $\phi_n := \Phi_n/\varphi_0$ . The phase is positive when it increases in the path across the junction from the upper electrode to the ground. The time derivative of the phase  $\phi_n$  is associated with the voltage  $V_n = -\varphi_0 \partial \phi_n / \partial t$  measured from the ground, where the minus sign indicates the direction of the phase. Under the Hamiltonian in Eq. (1), we derive the following

equation of motion of JTTL from Hamilton's equations:

$$\frac{\varphi_0 C_J}{I_c} \frac{\partial^2 \phi_n}{\partial t^2} - \frac{\varphi_0}{L I_c} (\phi_{n+1} - 2\phi_n + \phi_{n-1}) + \sin \phi_n = 0. \quad (2)$$

In the continuum limit, we take the lattice spacing  $\Delta x$  to be zero and promote the phase  $\phi_n$  to a field  $\phi(x, t)$  with circuit parameters per unit length  $c_J := C_J/\Delta x$ ,  $i_c := I_c/\Delta x$  and  $\ell := L/\Delta x$  being constant. Then, the equation of motion in Eq. (2) leads to the following sine-Gordon equation:

$$\partial_\tau^2 \phi(\xi, \tau) - \partial_\xi^2 \phi(\xi, \tau) + \sin \phi(\xi, \tau) = 0. \quad (3)$$

Here, we redefine the field  $\phi(\xi, \tau)$  as a function of the dimensionless coordinate  $\xi := x/\lambda_J$  and time  $\tau := \omega_p t$  using the Josephson penetration depth  $\lambda_J := \sqrt{\varphi_0/(\ell i_c)}$  and the plasma frequency  $\omega_p := \sqrt{i_c/(\varphi_0 c_J)}$ . Despite the nonlinearity of the sine-Gordon equation in Eq. (3), this is an integrable partial differential equation called a soliton equation, and we can find its exact solutions. One of solutions called a kink solution reads

$$\phi(\xi, \tau) = 4 \arctan \left[ \exp \left( \pm \frac{\xi - u_0 \tau - \xi_0}{\sqrt{1 - u_0^2}} \right) \right], \quad (4)$$

where the constant and dimensionless parameters  $u_0$  and  $\xi_0$  describe the velocity and the initial position of the kink, respectively. The parameters  $u_0$  and  $\xi_0$  are solely determined by the initial conditions of the kink. The sign  $\pm$  represents the polarity of the kink, which depends on the boundary condition of the system. Although we assume the plus sign for concrete calculations, an extension to the minus sign is straightforward. The dimensionless velocity  $u_0$  satisfies the inequality  $-1 < u_0 < 1$ , which means that the speed of the kink cannot exceed the velocity  $\bar{c} := \lambda_J \omega_p = 1/\sqrt{\ell c_J}$ . This the reason why  $\bar{c}$ , the Swihart velocity, is also called the *speed of light* of the JTTL.

For the kink solution of the plus polarity, we can calculate the voltage  $V(\xi, \tau) = -\varphi_0 \omega_p \partial \phi / \partial \tau$  measured from the ground, as

$$V(\xi, \tau) = \frac{\hbar \omega_p}{e} \frac{u_0}{\sqrt{1 - u_0^2}} \operatorname{sech} \left( \frac{\xi - u_0 \tau - \xi_0}{\sqrt{1 - u_0^2}} \right), \quad (5)$$

where the hyperbolic function  $\operatorname{sech}$  is defined as  $\operatorname{sech}(x) := 1/(\cosh(x)) = 2/(e^x + e^{-x})$ . The voltage pulse is called a single-flux-quantum (SFQ) pulse. Depending on the demensionless velocity  $u_0$ , the height and the width of the voltage pulse vary, respectively, while the time integral is conserved:

$$\int_{-\infty}^{\infty} dt V = 2\pi \varphi_0 \simeq 2.07 \times 10^{-15} \text{ Wb}. \quad (6)$$

This reflects the physical nature of the kink as a quantized magnetic flux, also called a fluxon.

We can apply a bias current  $I_b$  to each junction to modulate the velocity of the fluxon. Also, in practical circumstances, we have a finite amount of normal current across the junction, which is modeled by a resistor  $R_J$  shunting the junction (See Fig. 1). We introduce the conductance  $G_J = 1/R_J$  that quantifies the degree of normal current of the JTTL per unit cell, which gives rise to dissipation. Exploiting Kirchhoff's laws including those two circuit elements and taking the continuum limit with  $g_J = G_J/\Delta x$  and  $i_b = I_b/\Delta x$  being constant, we obtain the following perturbed sine-Gordon equation with bias and dissipation terms:

$$\partial_\tau^2 \phi - \partial_\xi^2 \phi + \sin \phi = \gamma - \alpha \partial_\tau \phi. \quad (7)$$

The dimensionless parameters are respectively defined as  $\alpha := g_J \sqrt{\varphi_0/(i_c c_J)}$  and  $\gamma := i_b/i_c$ , the former of which is called a damping coefficient. Although the surface loss of the upper electrode of the JTTL can be modeled by an additional term  $\beta \partial_\tau \xi \xi \phi$  to the right-hand side in Eq. (7), we assume that its contribution negligibly small in this study. One can add bias current to the JTTL spatially nonuniformly, and then the parameter  $\gamma$  is no longer a constant but a function  $\gamma(\xi)$  of the coordinate  $\xi$ , while we assume that it is constant otherwise mentioned.

One straightforward approach to solutions of the perturbed sine-Gordon equation is discretizing the space by a mesh of spacing  $a$  and numerically solving the following equations:

$$\partial_\tau^2 \phi_i - \frac{\lambda_J^2}{a^2} (\phi_{i+1} - 2\phi_i + \phi_{i-1}) + \sin \phi_i = \gamma_i - \alpha_i \partial_\tau \phi_i, \quad (8)$$

where  $\phi_i$  is the phase at each discretized point, and  $\gamma_i$  and  $\alpha_i$  can depend on the points, respectively. Although this method can incorporate the nonuniformities of the bias and the dissipation into the model, the numerical simulations are expensive and the results are not so clear to understand in a simple way.

## B. Perturbation theory of sine-Gordon equations

Another possible approach is resorting to the perturbation theory of sine-Gordon equations [66, 67], which is applicable to the situation where the bias and dissipation terms are small, i.e.  $|\gamma|, \alpha \ll 1$ , and we can treat them as perturbations. Then, we assume the perturbative kink solution of the phase field

$$\phi(\xi, \tau) = 4 \arctan \left[ \exp \left( \frac{\xi - \Xi(\tau)}{\sqrt{1 - u^2(\tau)}} \right) \right]. \quad (9)$$

The time-dependent functions  $u(\tau)$  and  $\Xi(\tau)$  describe the velocity and the centroid of the kink, respectively, and they are called modulation parameters. According to the perturbation theory of the sine-Gordon soliton, the bias and dissipation terms affect the dynamics of

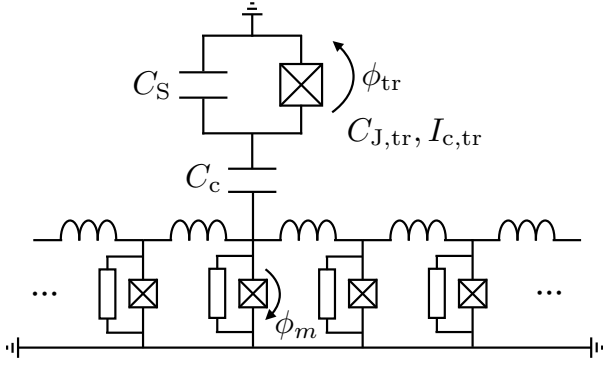


FIG. 2. Schematic diagram of a transmon capacitively coupled to a JTL. The transmon is characterized by the total capacitance  $C_{\Sigma} := C_S + C_{J,\text{tr}}$  —the summation of the shunt capacitance  $C_S$  and the transmon junction capacitance  $C_{J,\text{tr}}$ —and the critical current  $I_{c,\text{tr}}$  of the junction of the transmon. The transmon charging and Josephson energies  $E_{C,\text{tr}} := e^2/(2C_{\Sigma})$  and  $E_{J,\text{tr}} := \varphi_0 I_{c,\text{tr}}$  determine the properties of the transmon. The transmon is coupled to the  $m$ -th junction of the JTL via the coupling capacitor  $C_c$ .

the modulation parameters, which are governed by the following ordinary differential equations:

$$\frac{du}{d\tau} = -\frac{1}{4}\pi\gamma(1-u^2)^{\frac{3}{2}} - \alpha u(1-u^2), \quad (10)$$

$$\frac{d\Xi}{d\tau} = u. \quad (11)$$

Numerically solving the above differential equations is much more feasible compared with the aforementioned approach via direct discretization. We can derive the steady-state velocity  $u_{\text{ss}} := u(\infty)$  from the condition  $du/d\tau = 0$  in Eq. (10):

$$u_{\text{ss}} = -\text{sign}(\gamma) \left[ 1 + \left( \frac{4\alpha}{\pi\gamma} \right)^2 \right]^{-\frac{1}{2}}, \quad (12)$$

where  $\text{sign}(\gamma)$  takes 1 for  $\gamma > 0$  and  $-1$  for  $\gamma < 0$ . We observe that the balance between the bias and the dissipation determines the final velocity of the fluxon.

### C. Transmon

A transmon qubit [4] is typically made of a JJ shunted by a large capacitor that renders the qubit robust against charge noise from an environment (See Fig. 2). According to Kirchhoff's laws and the conventional quantization, we obtain the quantum Hamiltonian  $\hat{H}_{\text{tr}}$  of the transmon, as

$$\hat{H}_{\text{tr}} = 4E_{C,\text{tr}}\hat{n}_{\text{tr}}^2 - E_{J,\text{tr}}\cos\hat{\phi}_{\text{tr}}. \quad (13)$$

The charging energy  $E_{C,\text{tr}} := e^2/(2C_{\Sigma})$  is defined by the transmon capacitance as the summation  $C_{\Sigma} :=$

$C_{J,\text{tr}} + C_S$  of the shunt capacitance  $C_S$  and the junction capacitance  $C_{J,\text{tr}}$ , and  $E_{J,\text{tr}} := \varphi_0 I_{c,\text{tr}}$  denotes the Josephson energy of the transmon, where  $I_{c,\text{tr}}$  is the critical current. The Cooper-pair number and phase operators  $\hat{n}_{\text{tr}} := \hat{Q}_{\text{tr}}/(2e)$  and  $\hat{\phi}_{\text{tr}} := \hat{\Phi}_{\text{tr}}/\varphi_0$  denote the variables of the transmon, respectively, which satisfy the commutation relation  $[\hat{\phi}_{\text{tr}}, \hat{n}_{\text{tr}}] = i$ . After the conventional treatment [4, 28], we obtain the easily diagonalizable form of Hamiltonian under the condition  $E_{J,\text{tr}}/E_{C,\text{tr}} \simeq 50 \gg 1$ , as

$$\hat{H}_{\text{tr}} = (\hbar\omega_{\text{tr}} - E_{C,\text{tr}})\hat{a}^\dagger\hat{a} - \frac{E_{C,\text{tr}}}{2}\hat{a}^\dagger\hat{a}^\dagger\hat{a}\hat{a}, \quad (14)$$

where the bare transmon angular frequency reads  $\omega_{\text{tr}} := \sqrt{8E_{J,\text{tr}}E_{C,\text{tr}}}/\hbar$ . We introduced bosonic annihilation and creation operators  $\hat{a}$  and  $\hat{a}^\dagger$  satisfying the commutation relation  $[\hat{a}, \hat{a}^\dagger] = 1$ :

$$\hat{a} := \frac{1}{\sqrt{2}} \begin{pmatrix} \hat{\phi}_{\text{tr}} \\ \hat{\phi}_{0,\text{tr}} + i\frac{\hat{n}_{\text{tr}}}{n_{0,\text{tr}}} \end{pmatrix}. \quad (15)$$

The zero-point fluctuations of the phase and Cooper-pair number  $\phi_{0,\text{tr}} := (8E_{C,\text{tr}}/E_{J,\text{tr}})^{1/4}$  and  $n_{0,\text{tr}} := \{E_{J,\text{tr}}/(8E_{C,\text{tr}})\}^{1/4}$  are respectively defined. These expressions give us  $\sqrt{2}\hat{\phi}_{\text{tr}} = \phi_{0,\text{tr}}(\hat{a} + \hat{a}^\dagger)$  and  $\sqrt{2}\hat{n}_{\text{tr}} = -in_{0,\text{tr}}(\hat{a} - \hat{a}^\dagger)$ . We can diagonalize the transmon Hamiltonian in Eq. (14) by the Fock state  $|n\rangle$  such that  $\hat{a}^\dagger\hat{a}|n\rangle = n|n\rangle$  for non-negative integers  $n$ . Explicitly,

$$\hat{H}_{\text{tr}} = \sum_{n=0}^{\infty} E_n |n\rangle\langle n|, \quad (16)$$

$$E_n := \hbar\omega_{\text{tr}}n - \frac{E_{C,\text{tr}}}{2}n(n+1). \quad (17)$$

For the two-level approximation, we introduce the qubit states  $|\uparrow\rangle := |1\rangle$  and  $|\downarrow\rangle := |0\rangle$  of the transmon and truncate the higher excited states  $|2\rangle, |3\rangle, |4\rangle, \dots$  and so forth. Then, the Hamiltonian of the transmon is rewritten with respect to the Pauli operator acting only onto the qubit subspace, as

$$\hat{H}_{\text{tr}} = \frac{\hbar\omega_{\text{q}}}{2}\hat{\sigma}_z, \quad (18)$$

and we also have  $\sqrt{2}\hat{\phi}_{\text{tr}} = \phi_{0,\text{tr}}\hat{\sigma}_x$  and  $\sqrt{2}\hat{n}_{\text{tr}} = -n_{0,\text{tr}}\hat{\sigma}_y$ . Here, we define  $\hat{\sigma}_x := |\uparrow\rangle\langle\downarrow| + |\downarrow\rangle\langle\uparrow|$ ,  $\hat{\sigma}_y := -i|\uparrow\rangle\langle\downarrow| + i|\downarrow\rangle\langle\uparrow|$ , and  $\hat{\sigma}_z := |\uparrow\rangle\langle\uparrow| - |\downarrow\rangle\langle\downarrow|$ , and  $\omega_{\text{q}} := E_1/\hbar$  denotes the angular frequency of the transmon qubit under the two-level approximation. The Pauli matrices satisfy the commutation relations  $[\hat{\sigma}_\alpha, \hat{\sigma}_\beta] = 2i\sum_\gamma \epsilon_{\alpha\beta\gamma}\hat{\sigma}_\gamma$ , where  $\epsilon_{\alpha\beta\gamma}$  denotes the Edighnton's epsilon.

### D. JTL-transmon capacitive coupling

We consider a transmon capacitively coupled to a JTL via a coupling capacitor of capacitance  $C_c$  connecting

the transmon and the  $m$ -th junction of the JTL (See Fig. 2). Based on Kirchhoff's laws, we obtain the classical Hamiltonian of the total system, as

$$H = H_{\text{JTL}} + H_{\text{tr}} + H_{\text{int}}. \quad (19)$$

The newly introduced interaction Hamiltonian  $H_{\text{int}}$  explicitly reads

$$H_{\text{int}} := \frac{C_c}{C_J C_\Sigma} Q_m Q_{\text{tr}}. \quad (20)$$

We here promote the variables only for the transmon to the operators  $\hat{\phi}_{\text{tr}}$  and  $\hat{n}_{\text{tr}}$ . We treat the JTL classical mechanically due to the fact that for a typical low-impedance JTL satisfying  $Z_J := \sqrt{\ell/c_J} \ll R_Q := h/(2e)^2 \simeq 6.45 \text{ k}\Omega$ , which is the focus of the present paper, quantum fluctuations of the JTL are negligibly small [70–72]. In terms of the transmon operators, the quantum Hamiltonians acting onto the transmon degrees of freedom are written as

$$\begin{aligned} & \hat{H}_{\text{tr}} + \hat{H}_{\text{int}} \\ &= \sum_{n=0}^{\infty} E_n |n\rangle\langle n| - i\sqrt{2}en_{0,\text{tr}} \frac{C_c}{C_\Sigma C_J} Q_m (\hat{a} - \hat{a}^\dagger). \end{aligned} \quad (21)$$

### E. Circuit parameters

We assume the values of the circuit parameters of the total system, as shown in Table I. The values are typical for an long Josephson junction (LJJ) with the process rule of the critical current density  $j_c = 250 \text{ A/cm}^2$  and the capacitance per unit area  $C_{\text{area}} = 60 \text{ fF}/\mu\text{m}^2$ . The width  $w$  and the thickness  $b$  of the upper electrode and the length  $l$  of the LJJ are assumed to be  $w = 0.5 \mu\text{m}$ ,  $b = 0.3 \mu\text{m}$ , and  $l = 1.0 \text{ mm}$ , respectively. The inductance  $\ell$  per unit length is estimated by the formula of the geometric inductance  $\ell = (\mu_0/2\pi)[\ln(2l/r - 1)]$  for a circle wire of the radius  $r = \sqrt{wb}/\pi$ , where  $\mu_0 = 4\pi \times 10^{-7} \text{ H/m}$  denotes the permeability of free space. The value of the damping coefficient  $\alpha$  depends on the quality of the junction, the environmental temperature, the critical current density  $j_c$ , and so forth. Typical values of the damping coefficient of an underdamped LJJ is around  $\alpha \simeq 1.0 \times 10^{-3}$  [73, 74], whereas a large subgap resistance corresponding to the coefficient  $\alpha \simeq 1.3 \times 10^{-7}$  is reported for a small Al/AIO<sub>x</sub>/Al junction of area  $S = 23 \mu\text{m}^2$  at millikelvin temperature [75]. We assume the value from  $\alpha = 1.0 \times 10^{-6}$  to  $1.0 \times 10^{-3}$  for concrete calculations, and we leave its experimental realization for future work.

TABLE I. Circuit parameters used in the simulation.

Parameter	Symbol	Value
Inductance per unit length	$\ell$	$1.8 \times 10^{-6} \text{ H/m}$
Capacitance per unit length	$c_J$	$3.0 \times 10^{-8} \text{ F/m}$
Critical current per unit length	$i_c$	$1.25 \text{ A/m}$
Josephson penetration depth	$\lambda_J$	$12 \mu\text{m}$
Plasma frequency	$\omega_P$	$360 \text{ GHz}$
Capacitance of transmon	$C_\Sigma$	$100 \text{ fF}$
Critical current of transmon	$I_{c,\text{tr}}$	$20 \text{ nA}$
Josephson energy (devided by $h$ )	$E_{C,\text{tr}}/h$	$190 \text{ MHz}$
Charging energy (devided by $h$ )	$E_{J,\text{tr}}/h$	$9.9 \text{ GHz}$
Transmon qubit frequency	$\omega_q/(2\pi)$	$3.7 \text{ GHz}$
Coupling capacitance	$C_c$	$10 \text{ fF}$
Dimensionless coupling constant	$\eta_c$	$2.9 \times 10^{-3}$

## III. TIME-DELAY READOUT OF A TRANSMON QUBIT

### A. Perturbative effect on JTL induced by transmon qubit under the two-level approximation

Under the two-level approximation of the transmon, the Hamiltonians acting onto the transmon qubit subspace are expressed by the Pauli matrices, as

$$\hat{H}_{\text{tr}} + \hat{H}_{\text{int}} = \frac{\hbar\omega_q}{2} \hat{\sigma}_z + \hbar g_c(t) \hat{\sigma}_y. \quad (22)$$

Here, we define the coupling amplitude

$$g_c(t) := -\sqrt{2} n_{0,\text{tr}} \frac{e}{\hbar} \frac{C_c}{C_\Sigma C_J} Q_m(t), \quad (23)$$

which is related to the voltage of the  $m$ -th junction  $V_m(t) = -Q_m(t)/C_J$  measured from the ground. To derive an effective Hamiltonian for a weak coupling  $|g_c(t)| \ll \omega_q$ , we exploit the Schrieffer–Wolff (SW) transformation. Then, we obtain the following effective Hamiltonian for a weak coupling with a slowly moving fluxon of the initial velocity  $u_0$  satisfying  $u_0 \ll \omega_q/\omega_P$  (See Appendix A 2):

$$\hat{H}_{\text{SW}}(t) \simeq \frac{\hbar\omega_q}{2} \hat{\sigma}_z + \frac{\hbar g_c^2(t)}{\omega_q} \hat{\sigma}_z. \quad (24)$$

The second term on the right-hand side of Eq. (24) is the effective perturbation term of the JTL. This result corresponds to that derived from the adiabatic approximation adopted for inductive coupling between a JTL and a flux qubit at the symmetry point [55]. Also, we note that the qubit free part in the first term of Eq. (24) and the effective perturbation term commute, which is the feature of the non-demolition readout [17, 28]. The degree of nonadiabatic state transitions caused by the fluxon is evaluated in subsection III D.

Because the transmon parts are now written solely by the Pauli operator  $\hat{\sigma}_z$ , we treat  $\hat{\sigma}_z$  as a c-number  $\sigma_z$  that takes  $+1$  for  $|\uparrow\rangle$  and  $-1$  for  $|\downarrow\rangle$ . Then, after the fluxon-qubit scattering, the total Hamiltonian in the original

frame reads

$$\begin{aligned} H &= H_{\text{JTL}} + H_{\text{SW}}(t) \\ &= H_{\text{JTL}} + 2n_{0,\text{tr}}^2 \frac{e^2}{\hbar\omega_q} \frac{C_c^2}{C_\Sigma^2 C_J^2} Q_m^2 \sigma_z + \frac{\hbar\omega_q}{2} \sigma_z. \end{aligned} \quad (25)$$

Only retaining the Hamiltonians regarding the JTL, we obtain the modified classical Hamiltonian  $H'_{\text{JTL}}$  that describes a perturbed dynamics of JTL by the transmon qubit, as

$$H'_{\text{JTL}} := H_{\text{JTL}} + 2n_{0,\text{tr}}^2 \frac{e^2}{\hbar\omega_q} \frac{C_c^2}{C_\Sigma^2 C_J^2} Q_m^2 \sigma_z. \quad (26)$$

The perturbation term is nothing but a local change in the capacitance of JTL's junction labeled by  $m$ , and thus the resulting sine-Gordon equation involves an additional term proportional to  $\partial_\tau^2 \phi_m$ . In the continuum limit, we obtain

$$\partial_\tau^2 \phi + \alpha \partial_\tau \phi - \partial_\xi^2 \phi + \sin \phi = \eta_c \delta(\xi) \sigma_z \partial_\tau^2 \phi, \quad (27)$$

where we set the origin of coordinate  $\xi$  to be the position of the  $m$ -th junction of the JTL (See Appendix B 1). The dimensionless constant  $\eta_c \ll 1$  of the capacitive coupling is defined as

$$\eta_c := \frac{1}{1-p} \frac{C_c^2}{\lambda_J c_J C_\Sigma}, \quad (28)$$

where  $p$  is a dimensionless constant:

$$p := \sqrt{\frac{E_{C,\text{tr}}}{8E_{J,\text{tr}}}} = \frac{1}{8} \phi_{0,\text{tr}}^2. \quad (29)$$

For a typical transmon with  $E_{J,\text{tr}}/E_{C,\text{tr}} \simeq 50$ ,  $p \simeq 1/20$ .

## B. Time delay of fluxons

We analytically calculate the time delay between the scattered fluxons for  $|\uparrow\rangle$  and  $|\downarrow\rangle$ . Based on the perturbation theory of the sine-Gordon kink [66, 67], the velocity  $u(\tau)$  and centroid  $\Xi(\tau)$  in the perturbed kink in Eq. (9) obey the following ordinary differential equations (See Appendix B 3):

$$\frac{du}{d\tau} = -\alpha u(1-u^2) - \frac{1}{2} \eta_c \sigma_z u^2 \text{sech}^3(\Theta_0) \sinh(\Theta_0), \quad (30)$$

$$\frac{d\Xi}{d\tau} = u + \frac{1}{2} \eta_c \sigma_z \frac{u^3}{\sqrt{1-u^2}} \Theta_0 \text{sech}^3(\Theta_0) \sinh(\Theta_0), \quad (31)$$

where we do not apply bias current to the JTL. Here, we introduced the time-dependent function  $\Theta_0$ , as

$$\Theta_0(\tau) := \frac{\Xi(\tau)}{\sqrt{1-u^2(\tau)}}. \quad (32)$$

We consider the situation in which a moving fluxon of the initial velocity  $u_0$  is scattered by the transmon qubit in the state  $|\uparrow\rangle$  or  $|\downarrow\rangle$ . Then, the modulated velocity  $u(\tau)$  and centroid  $\Xi(\tau)$  are related with each other as

$$\sqrt{\frac{1-u^2}{1-u_0^2}} = 1 - \frac{1}{4} \eta_c \sigma_z \frac{u_0^2}{\sqrt{1-u_0^2}} \text{sech}^2(\Theta_0), \quad (33)$$

where we assumed that the transmon-JTL interaction is more dominant compared with the dissipation (See Appendix B 4). Namely, we assume that

$$\alpha \ll \eta_c u_0. \quad (34)$$

For a fluxon propagating to the positive direction, i.e.  $u > 0$ , we can solve Eq. (33) for  $u$  and obtain

$$u(\Xi) \simeq u_0 \left[ 1 + \frac{1}{4} \eta_c \sigma_z \sqrt{1-u_0^2} \text{sech}^2 \left( \frac{\Xi}{\sqrt{1-u_0^2}} \right) \right], \quad (35)$$

where we neglected the higher-order terms.

Now, we are ready to analytically calculate the time delay of the fluxon induced by the transmon qubit under the two-level approximation. Comparing the propagation times  $\tau_{|\uparrow\rangle}$  and  $\tau_0$ , which respectively represent the propagation time under the capacitive coupling to the transmon qubit in the state  $|\uparrow\rangle$  and under no coupling, we calculate

$$\begin{aligned} \tau_{|\uparrow\rangle} - \tau_0 &:= \int_{-\infty}^{\infty} d\Xi \left( \frac{1}{u(\Xi)} - \frac{1}{u_0} \right) \Big|_{\sigma_z=+1} \\ &\simeq -\eta_c \frac{\sqrt{1-u_0^2}}{4u_0} \int_{-\infty}^{\infty} d\Xi \text{sech}^2 \left( \frac{\Xi}{\sqrt{1-u_0^2}} \right) \\ &= -\eta_c \frac{1-u_0^2}{2u_0}. \end{aligned} \quad (36)$$

We evaluated the integral by the method of residues. The result means that the capacitive coupling with the transmon qubit in the state  $|\uparrow\rangle = |1\rangle$  accelerates the fluxon. Similarly,

$$\tau_{|\downarrow\rangle} - \tau_0 = \eta_c \frac{1-u_0^2}{2u_0}, \quad (37)$$

which means that the transmon qubit in  $|\downarrow\rangle = |0\rangle$  decelerates the fluxon. Comparing the cases for  $|\uparrow\rangle$  and  $|\downarrow\rangle$ , the dimensionless time delay  $\tau_d := \tau_{|\downarrow\rangle} - \tau_{|\uparrow\rangle}$  reads

$$\tau_d \simeq \eta_c \frac{1-u_0^2}{u_0} = \frac{1-u_0^2}{u_0(1-p)} \frac{C_c^2}{\lambda_J c_J C_\Sigma}. \quad (38)$$

Recovering the dimension of time  $\omega_p^{-1}$ , we end up with the time delay  $T_d$  in a unit of time, as

$$T_d := \tau_d \omega_p^{-1} \simeq \frac{1-u_0^2}{u_0(1-p)} \frac{C_c^2}{C_\Sigma} Z_J, \quad (39)$$

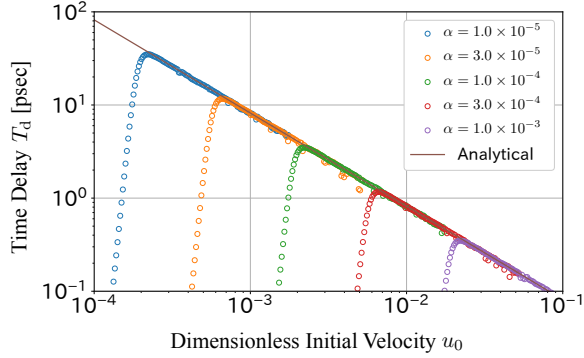


FIG. 3. (circles) Numerical results of the time delay  $T_d = (\tau_{|\downarrow\rangle} - \tau_{|\uparrow\rangle})\omega_p^{-1}$  calculated by numerically solving Eqs. (30) and (31) for several values of the damping coefficient  $\alpha$  and (line) analytical result in Eq. (39). We adopt the values of circuit parameters in Table I.

where  $Z_J = \sqrt{\ell/c_J}$  denotes the characteristic impedance of the JTL. This expression illustrates one important consequence that the fluxon initial velocity  $u_0$  is a knob that we can control to enhance the time delay without changing the device parameters. We also observe that we can enhance the time delay by utilizing a JTL of a large characteristic impedance  $Z_J$ , which can be increased by exploiting the upper electrode made of high-kinetic-inductance materials [72].

In Fig. 3, we provide numerical results of the time delay  $T_d$ , obtained by numerically solving the differential equations of the modulation parameters in Eqs. (30) and (31). The values of parameters are presented in Table I. For varied fluxon initial velocity  $u_0$ , we confirm good agreements with the analytical results for small values of damping coefficient  $\alpha$ . However, as  $\alpha$  increases, the numerical results deviate from the analytical one below the threshold velocity, which increases with  $\alpha$ . This reflects the violation of the assumption in Eq. (34). Therefore, a small damping coefficient is advantageous for obtaining a large amount of time delay.

### C. Absence of fluxon pinning

As is done in the previous studies [55, 68], we examine the fluxon pinning effect induced by the transmon qubit capacitively coupled to the JTL. When the fluxon pinning occurs, the velocity satisfies  $u = 0$  at a certain position of centroid  $\Xi$ . Supposing this condition in Eq. (33) leads us to

$$\text{sech}^2 \Xi = -\frac{2}{\eta_c} \sigma_z, \quad (40)$$

where we neglected the higher-order terms  $O(\eta_c^2)$ . Therefore, under the condition of the perturbation theory  $\eta_c \ll 1$ , the pinning condition above cannot be held for any  $\Xi \in \mathbb{R}$  regardless of the value of  $\sigma_z$ . We thus

conclude that the fluxon pinning is absent for weak capacitive coupling between the transmon qubit and JTL, which is distinct feature from that for inductive coupling [55, 68].

### D. Nonadiabatic transition

We recall the Hamiltonian of the transmon qubit under the two-level approximation driven by the moving fluxon in Eq. (22),  $\hat{H}(t) = \hat{H}_0 + \hat{V}(t)$ , where  $\hat{H}_0 := (\hbar\omega_q/2)\hat{\sigma}_z$  and  $\hat{V}(t) := \hbar g_c(t)\hat{\sigma}_y$ . Because the driving term proportional to  $\hat{\sigma}_y$  does not commute with the energy basis  $\hat{\sigma}_z$  of the transmon, we expect nonadiabatic transitions between  $|\uparrow\rangle$  and  $|\downarrow\rangle$  induced by the driving. The profile of the coupling amplitude  $g_c(t)$  is explicitly given as

$$g_c(t) = \sqrt{2}n_{0,\text{tr}} \frac{C_c}{C_\Sigma} \frac{u_0\omega_p}{\sqrt{1-u_0^2}} \text{sech} \left[ \frac{u_0\omega_p t + \xi_0}{\sqrt{1-u_0^2}} \right]. \quad (41)$$

Here, the origin  $\xi = 0$  denotes the position of the transmon qubit and  $\xi_0$  is defined as the initial position of fluxon's centroid.

Based on Fermi's golden rule applicable for a weak coupling  $|g_c(t)| \ll \omega_q$ , we can calculate the probabilities  $P(\uparrow|\downarrow)$  and  $P(\downarrow|\uparrow)$  of the transitions  $|\downarrow\rangle \mapsto |\uparrow\rangle$  and  $|\uparrow\rangle \mapsto |\downarrow\rangle$  respectively, as

$$P(\uparrow|\downarrow) \simeq \frac{1}{\hbar^2} \left| \int_{-\infty}^{\infty} ds e^{i\omega_q s} \langle \uparrow | \hat{V}(s) | \downarrow \rangle \right|^2, \quad (42)$$

$$P(\downarrow|\uparrow) \simeq \frac{1}{\hbar^2} \left| \int_{-\infty}^{\infty} ds e^{-i\omega_q s} \langle \downarrow | \hat{V}(s) | \uparrow \rangle \right|^2. \quad (43)$$

Utilizing the expression of  $\hat{V}(s)$  and the formula

$$\int_{-\infty}^{\infty} dx e^{ikx} \text{sech}(ax) = \frac{\pi}{|a|} \text{sech} \left( \frac{\pi k}{2a} \right), \quad (44)$$

we obtain

$$\begin{aligned} P(\uparrow|\downarrow) &= P(\downarrow|\uparrow) \\ &= 2\pi^2 n_{0,\text{tr}}^2 \frac{C_c^2}{C_\Sigma^2} \text{sech}^2 \left( \frac{\pi}{2} \frac{\sqrt{1-u_0^2} \omega_q}{u_0 \omega_p} \right). \end{aligned} \quad (45)$$

From this result, the nonadiabatic transitions are exponentially suppressed under the following condition on the fluxon initial velocity  $u_0$ :

$$\frac{\sqrt{1-u_0^2}}{u_0} \gg \frac{2\omega_p}{\pi\omega_q}. \quad (46)$$

In practical situations, the ratio is approximated as

$$\frac{2\omega_p}{\pi\omega_q} \simeq \frac{2 \times 360 \text{ GHz}}{\pi \times 2\pi \times 3.7 \text{ GHz}} \simeq 9.9 \quad (47)$$

and thus the nonadiabatic transitions are negligibly small for the fluxon initial velocity  $u_0 < 0.01$ , as is assumed to yield an enough amount of the time delay. In

our scheme employing the capacitive coupling, we can decrease the initial velocity of fluxon without suffering from the pinning caused by the coupling to the qubit, and thereby we can enhance the delay time and suppress the nonadiabatic transitions at the same time.

### E. Pulse separation via bias current

Whereas we can increase the time delay  $\tau_d$ , namely the temporal width of delay, by modulating the fluxon initial velocity  $u_0$ , the dimensionless spatial width of delay  $\Delta\xi_d := u_0\tau_d$  is constant under the change in  $u_0$ :

$$\Delta\xi_d \simeq \eta_c \ll 1. \quad (48)$$

The unit of coordinate  $\xi$  was  $\lambda_J$  that is the spatial width of a slow fluxon, thus the scattered fluxons for  $|\downarrow\rangle$  and  $|\uparrow\rangle$  are almost completely overlapped each other, which makes it hard to detect the delay between them at the subsequent stage. We could bump the fluxon  $N_{\text{int}}$  times into the transmon and obtain  $N_{\text{int}}$  times larger spatial width of delay  $\Delta\xi_{d,\text{tot}} = N_{\text{int}}\eta_c$  by exploiting an annular LJJ [76, 77].

We here propose another approach based on bias current after the fluxon scattering. We concretely consider the following sine-Gordon equation in which a nonuniform bias current  $\gamma(\xi)$  is applied:

$$\partial_\tau^2\phi - \partial_\xi^2\phi + \sin\phi = \gamma(\xi) - \alpha\partial_\tau\phi. \quad (49)$$

In spite of the nonuniform bias term, the equation of motion preserves the time-translation symmetry; if a function  $\phi = \phi(\xi, \tau)$  is a solution of Eq. (49), then another temporally delayed function  $\phi_d(\xi, \tau) = \phi(\xi, \tau - \tau_d)$  is also a solution of Eq. (49). This means that the time delay  $\tau_d$  is preserved before and after the nonuniform bias  $\gamma(\xi)$ . On the other hand, the space-translation symmetry is violated due to the nonuniform bias, and thus the spatial width of delay is not preserved. For simplicity, we consider the bias profile  $\gamma(\xi)$  such that  $\gamma(\xi) = 0$  for  $0 \leq \xi < \xi_b$  and  $\gamma(\xi) = \gamma = \text{const.}$  for  $\xi_b \leq \xi$ , where  $\xi_b$  denotes starting point of the biased region. After the accelerated fluxon reaches the steady-state velocity in Eq. (12), the spatial width of the fluxon becomes  $\sqrt{1 - u_{\text{ss}}^2}$ . Comparing the spatial width  $\sqrt{1 - u_{\text{ss}}^2}$  of the accelerated fluxon and the amplified spatial width of delay  $u_{\text{ss}}\tau_d$ , we find the condition on the absolute value of the bias  $|\gamma|$  for significant separation of the two fluxons for  $|\downarrow\rangle$  and  $|\uparrow\rangle$ :

$$|\gamma| \gg \frac{\alpha u_0}{\eta_c}. \quad (50)$$

We neglected the constant  $4/\pi$  that is irrelevant to the order estimation.

We numerically examine the effect of nonuniform bias current for pulse separation, as shown in Fig. 4. The figure shows numerically obtained snapshots of accelerated fluxons by a nonuniform bias current  $\gamma(\xi)$ , where

its value is  $\gamma(\xi) = -0.1$  at the biased region for  $\xi \geq \xi_b$  and  $\gamma = 0$  for  $0 \leq \xi < \xi_b$ , and  $\xi_b = 15$ . We plot the dynamics of two fluxons with the same initial velocity  $u_0 = 0.01$  and different initial positions of centroid  $\xi_0 = 5.75$  and  $5.85$ , and thus the spatial width of delay is  $\Delta\xi_d = 0.1$ . See Eq. (4) for an explicit expression of the initial fluxons. As is seen in the magnified plot at  $\tau = 300$  (inset), the two fluxons are almost completely overlapped before the acceleration. After the acceleration, the spatial width between the two fluxons are amplified, and the pluses are contracted. Whereas the pulses collapse after the acceleration around  $\tau = 410$ , this can be suppressed by increasing the number of discretized points for the numerical calculations, and thus we expect that the pulse collapse is not observed in an LJJ.

### F. Detection of time delay based on SFQ digital circuits

RSFQ digital circuits operating at several tens of gigahertz [39] are suitable for detecting time delays. The operating frequency of RSFQ circuits roughly increases in proportion to the square root of the critical current density. However, since it becomes difficult to fabricate Josephson junctions with small critical current values in a high critical current density process, there is a trade-off with power consumption. We assume that the appropriate critical current density is in the range of  $0.1\text{--}1.0\text{ kA/cm}^2$ , which allows us to achieve  $5\text{--}20\text{ GHz}$  operation. We can enhance the time resolution beyond the operation frequency by exploiting time delay detection techniques, such as prescaler circuits. For example, an SFQ time-to-digital converter with a time resolution of 5 picoseconds or less was demonstrated, with a critical current density of  $1\text{ kA/cm}^2$  at  $4.2\text{ K}$  [78], where thermal noise is dominant at this temperature [79]. Hence, we can digitize the information of the qubit state within low-temperature stages by detecting the time delay exceeding the time resolution around 5 picoseconds, as demonstrated in Fig. 3. Also, as is estimated by the numerical calculations, the height of the voltage pulse after the fluxon acceleration is around one millivolt that is manageable by SFQ digital circuits. We raise related studies for time delay detection based on SFQ circuits that we can potentially employ [60, 80–84].

## IV. TIME-DELAY READOUT OF A MULTI-LEVEL TRANSMON

### A. Perturbative effect on JTL induced by multi-level transmon

We now extend the scope to a multi-level transmon without the two-level approximation. Recalling the Hamiltonians in Eq. (21) regarding a multi-level transmon capacitively coupled with a JTL, we derive the SW-

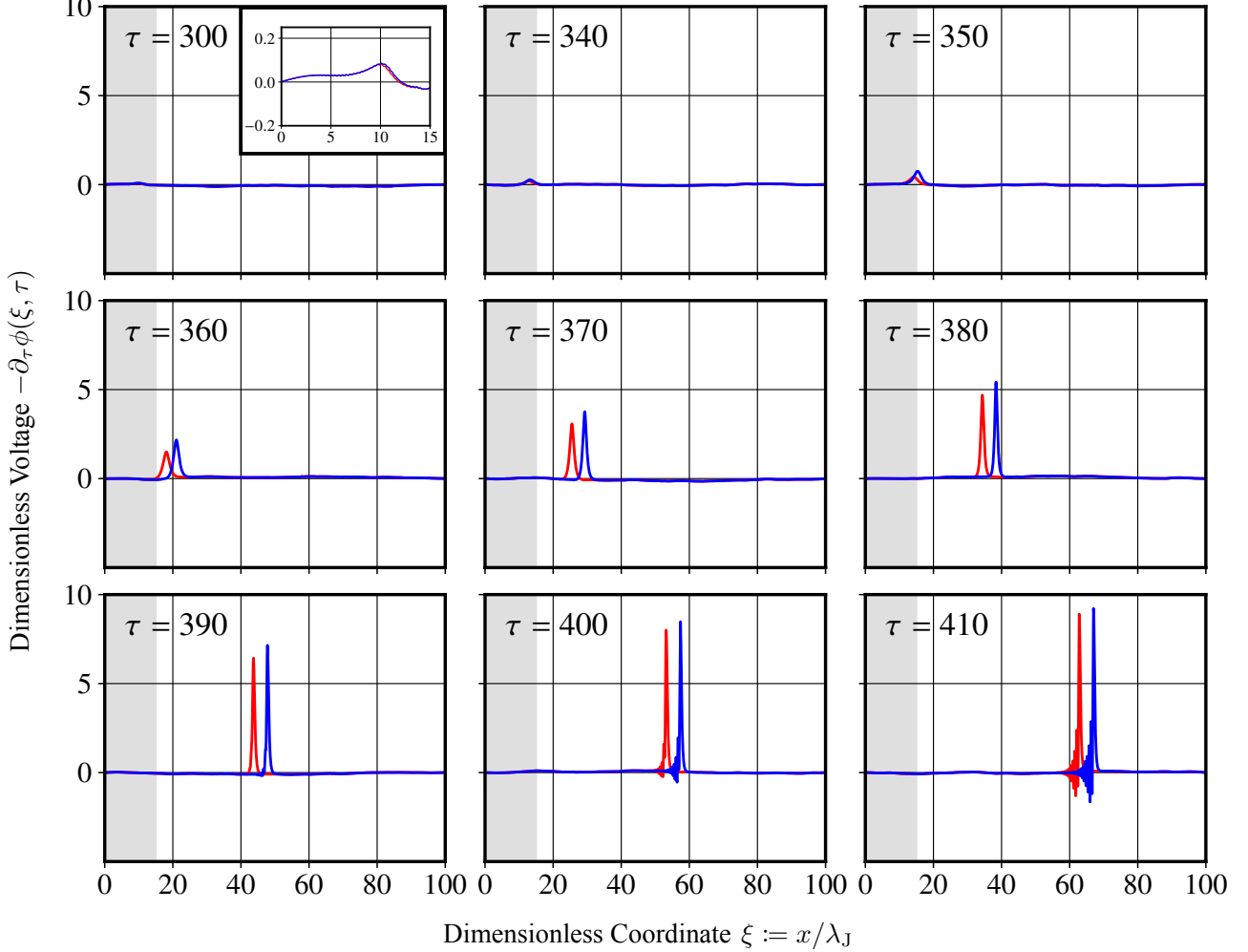


FIG. 4. Numerically obtained snapshots of accelerated fluxons as dimensionless voltage pulses  $V(\xi, \tau)/(\varphi_0 \omega_p) = -\partial_\tau \phi(\xi, \tau)$  for two different initial positions of centroid  $\xi_0 = 5.75$  and  $5.85$ . The grey area satisfying  $0 \leq \xi < 15$  represents the nonbiased region, while the white area satisfying  $\xi \geq 15$  represents the biased region by the dimensionless bias  $\gamma = -0.1$ . The initial velocity is  $u_0 = 0.01$  for both cases, and the damping coefficient is  $\alpha = 1.0 \times 10^{-6}$ . We assume the closed boundary conditions at the ends of the JTL, i.e.  $\phi(0, \tau) = 0$  and  $\phi(100, \tau) = 2\pi$  for an arbitrary time  $\tau$ . When we assume the values of circuit parameters in Table I, the unities of time  $\tau$ , coordinate  $\xi$ , and voltage are 2.8 ps,  $12 \mu\text{m}$ , and 0.12 mV, respectively.

transformed effective Hamiltonian:

$$\hat{H}_{\text{SW}} \simeq \hat{H}_{\text{tr}} - \sum_n \frac{C_c^2 Q_m^2 / (2C_J^2 C_\Sigma)}{[1 - np][1 - (n+1)p]} |n\rangle \langle n|, \quad (51)$$

where we omit off-diagonal terms that are negligible for a small-photon-number state  $|n\rangle$  (See Appendix A 3). The effective perturbation Hamiltonian commutes with the free part  $\hat{H}_{\text{tr}}$ , and thus the photon-number (Fock) state is not destroyed, which demonstrates the non-demolition readout [28]. The perturbation can be attributed to the change in the capacitance of the  $m$ -th junction of the JTL

$$C_J \mapsto C_J + \frac{C_c^2 / C_\Sigma}{[1 - np][1 - (n+1)p]}, \quad (52)$$

which depends on the photon-number (Fock) state  $|n\rangle$  of the multi-level transmon without the two-level approximation. We then derive the dimensionless constant  $\eta_{c,\text{tr}} = \eta_{c,\text{mlt}}(|n\rangle)$  that depends on the photon number  $n$ , as (See Appendix B 2)

$$\eta_{c,\text{mlt}}(|n\rangle) = \frac{-1}{[1 - np][1 - (n+1)p]} \frac{C_c^2}{\lambda_J c_J C_\Sigma}. \quad (53)$$

## B. Time delay of fluxons

As is evaluated for a transmon qubit under the two-level approximation, we derive an expression for the propagation time  $\tau_{|n\rangle}$  compared with that in the ab-

sence of coupling  $\tau_0$ , as

$$\tau_{|n\rangle} - \tau_0 \simeq \frac{C_c^2/(\lambda_J c_J C_\Sigma)}{[1 - np][1 - (n+1)p]} \frac{1 - u_0^2}{2u_0}. \quad (54)$$

We therefore end up with the difference of the propagation times between the cases for  $|n\rangle$  and  $|n+1\rangle$ , as

$$\tau_{|n\rangle} - \tau_{|n+1\rangle} \simeq \frac{-(1 - u_0^2)pC_c^2/(\lambda_J c_J C_\Sigma)}{u_0[1 - np][1 - (n+1)p][1 - (n+2)p]}. \quad (55)$$

Especially for  $n = 0$ ,

$$T_{|0\rangle} - T_{|1\rangle} \simeq -\frac{p}{1 - 2p} \frac{1 - u_0^2}{u_0(1 - p)} \frac{C_c^2}{C_\Sigma} Z_J, \quad (56)$$

where the dimension of time is recovered. Due to the factor  $-p/(1 - 2p)$ , the result does not reproduce the result in Eq. (39) obtained via the two-level approximation followed by the SW transformation. The factor decreases the time delay for a typical transmon as  $p \simeq 1/20$ , which is a negative result for one to increase the time delay. We also face a similar degradation of the dispersive shift due to small anharmonicity of a multi-level transmon [28]. The degradation of time delay should be compensated by slowing the fluxon initial velocity  $u_0$  or increasing the characteristic impedance  $Z_J$  of the JTTL.

### C. Absence of fluxon pinning

Regarding the fluxon pinning, the same discussion as that for a transmon qubit under the two-level approximation can be applied, and thus the pinning does not occur even for the multi-level transmon capacitively coupled to the JTTL.

### D. Nonadiabatic transition

We evaluate the effects of nonadiabatic transitions between the transmon energy eigenstates, namely, the photon-number (Fock) states  $|n\rangle$ . Again, recalling the Hamiltonian of the multi-level transmon in Eq. (21), the transition probability from  $|n_i\rangle$  to  $|n_f\rangle$  is calculated as

$$P(n_f|n_i) = \frac{1}{\hbar^2} \left| \int_{-\infty}^{\infty} ds e^{\frac{i}{\hbar}(E_{n_f} - E_{n_i})s} \langle n_f | \hat{V}(s) | n_i \rangle \right|^2, \quad (57)$$

according to Fermi's golden rule. For the Hamiltonian  $\hat{V}(t) := i\hbar g_c(t)(\hat{a} - \hat{a}^\dagger)$ , only transitions between neighbouring photon-number states are allowed, which is because Fermi's golden rule is second-order perturbative. The transition probabilities of  $|n_i\rangle \mapsto |n_i + 1\rangle$  and

$|n_i\rangle \mapsto |n_i - 1\rangle$  are explicitly evaluated, respectively, as

$$P(n_i + 1|n_i) = (n_i + 1) \left| \int_{-\infty}^{\infty} ds e^{i\omega_{n_i+1}s} g_c(s) \right|^2, \quad (58)$$

$$P(n_i - 1|n_i) = n_i \left| \int_{-\infty}^{\infty} ds e^{-i\omega_{n_i}s} g_c(s) \right|^2, \quad (59)$$

where  $\omega_n = (E_n - E_{n-1})/\hbar$  denotes the angular frequency of the subspace spanned by the neighbouring photon-number states  $|n\rangle$  and  $|n-1\rangle$ . Putting the expression in Eq. (41) and exploiting the formula in Eq. (44), we end up with

$$\begin{aligned} P(n_i + 1|n_i) &= 2(n_i + 1)\pi^2 n_{0,\text{tr}}^2 \frac{C_c^2}{C_\Sigma^2} \text{sech}^2 \left( \frac{\pi}{2} \frac{\sqrt{1 - u_0^2} \omega_{n_i+1}}{u_0 \omega_p} \right), \end{aligned} \quad (60)$$

$$\begin{aligned} P(n_i - 1|n_i) &= 2n_i \pi^2 n_{0,\text{tr}}^2 \frac{C_c^2}{C_\Sigma^2} \text{sech}^2 \left( \frac{\pi}{2} \frac{\sqrt{1 - u_0^2} \omega_{n_i}}{u_0 \omega_p} \right). \end{aligned} \quad (61)$$

These results resemble the result in Eq. (45), while the prefactors  $n_i + 1$  and  $n_i$  are present due to coefficients of bosonic operators. As is shown in the discussion of the transmon qubit under the two-level approximation, we conclude that the nonadiabatic transitions are negligible even for a multi-level transmon when we are interested in the photon-number state  $|n\rangle$  that satisfies

$$\frac{\pi}{2} \frac{\sqrt{1 - u_0^2} \omega_{n+1}}{u_0 \omega_p} \gg 1. \quad (62)$$

Thus, decreasing the fluxon initial velocity  $u_0$  allows for the exponential suppression of the nonadiabatic transitions between the photon-number states of the multi-level transmon.

## V. RADIATIVE DECAY INDUCED BY JTTL

### A. Klein-Gordon transmission line (KGTL)

To evaluate the degree of radiative decay mediated by a JTTL, we work on a transmon capacitively coupled to a JTTL at one end, and the other end is terminated by an external apparatus controlling input or output signals (See Fig. 5 (a)). We here rely on a harmonic approximation of the JTTL; we replace the JJs in the JTTL by linear inductors, whose inductance  $L_J$  per unit cell is related to the critical current  $I_c$  of the junctions, as  $L_J := \varphi_0/I_c$  (See Fig. 5 (b)). To take the continuum limit consistently, we take the limit  $\Delta x \rightarrow 0$  with the parameter  $\zeta_J := L_J \Delta x$  being constant. This harmonic approximation is nothing but the truncation of the cosine potential, as  $-\cos \phi \simeq -1 + (1/2)\phi^2$ , and neglecting the constant  $-1$ . This is based on the observation

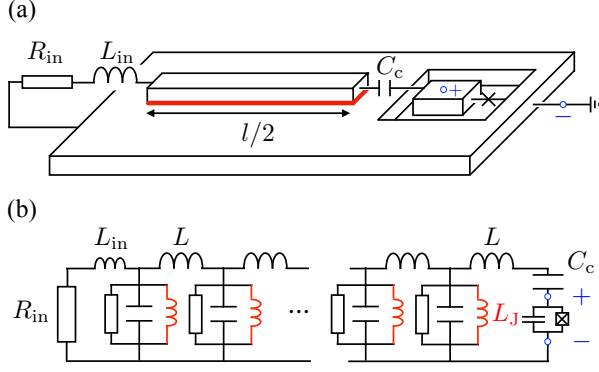


FIG. 5. (a) A transmon capacitively coupled to a JTL at one end via a coupling capacitor  $C_c$ , and the other end is terminated by an external source made of a resistor  $R_{in}$  and an inductor  $L_{in}$ . The red region represents the JTL in which a fluxon propagates. (b) A lumped-element circuit diagram of the system. The junctions in the JTL are approximated by inductors  $L_J$ , where the Josephson energy  $E_J$  and the corresponding inductance  $L_J$  are associated with each other, as  $L_J := \varphi_0^2/E_J = \varphi_0/I_c$  per unit cell of the JTL. The approximated transmission line is called a KGTL. The small square represents a subgap resistor  $R_J$  per unit cell. Other parameters are the same as the previous ones.

that the dynamics of a low-impedance JTL possessing no fluxon is well captured only by small-amplitude oscillations around the potential minimum  $\phi \simeq 0$ . We then obtain the following Klein–Gordon equation to be obeyed:

$$\partial_\tau^2 \phi - \partial_\xi^2 \phi + \phi = 0, \quad (63)$$

where we at the moment omit the dissipation. Recovering the dimensions of coordinate and time, the dispersion relation of the Klein–Gordon transmission line (KGTL) reads

$$\omega^2(k) = \omega_p^2 + \bar{c}^2 k^2. \quad (64)$$

The spectral gap  $\omega_p$  is rooted in the mass term  $\phi$  appearing in the Klein–Gordon equation in Eq. (63), and this is reminiscent of a bandgap in a structured waveguide [85, 86]. We expect from the dispersion relation that radiative decay of the qubit having an angular frequency around  $\omega_q \simeq 2\pi \times 3.7$  GHz is strongly suppressed by the intrinsic spectral gap  $\omega_p \simeq 360$  GHz.

## B. Radiative decay induced by KGTL

We calculate the radiative decay rate induced by a dissipationless KGTL of length  $l/2$  (See Fig. 5 (a) for an image of the JTL-transmon system and Fig. 5 (b) for an approximated circuit diagram). Owing to the electrical circuit theory (See Appendix C1), we obtain an analytical expression of the radiative decay rate  $\gamma(\omega_q)$  of the capacitively coupled transmon at one end of the

KGTL that is terminated by an external impedance  $Z_0 := R_{in} + i\omega L_{in}$  at the other end:

$$\gamma(\omega_q) \simeq \frac{2\text{Re} \left[ i \frac{\tilde{Z}_J(\omega_q) \{Z_0^2 + \tilde{Z}_J^2(\omega_q)\}}{\{Z_0 + i\tilde{Z}_J(\omega_q)\}^2} \right]}{C_\Sigma \left[ \tilde{Z}_J(\omega_q) - 1/(\omega_q C_c) \right]^2} e^{-l/\lambda_J}. \quad (65)$$

This result demonstrates the exponential suppression of the radiative decay mediated by the dissipationless KGTL. We here introduced an effective impedance of KGTL  $\tilde{Z}_J(\omega) := Z_J/\sqrt{(\omega_p^2/\omega^2) - 1}$  and assumed the conditions  $\omega_q < \omega_p$  and  $\lambda_J \ll l$  applicable for typical systems. For a simple expression, we consider the situation in which  $L_{in} = 0$  and  $\tilde{Z}_J(\omega_q) \ll R_{in}, 1/(\omega_q C_c)$ . Then, we arrive at (See Appendix C2)

$$\gamma(\omega_q) \simeq 4\omega_q^2 \frac{C_c^2}{C_\Sigma} \frac{\tilde{Z}_J^2(\omega_q)}{R_{in}} e^{-l/\lambda_J}. \quad (66)$$

In a practical circumstance, the JTL contains a finite amount of normal leakage current described by intrinsic shunt resistors, also depicted in Fig. 5 (a) and (b). Under the conditions  $\omega_q < \omega_p$  and  $\lambda_J \ll l$ , we eventually obtain

$$\gamma(\omega_q) \simeq \alpha \frac{\omega_q^3}{2\omega_p} \frac{C_c^2}{C_\Sigma} \tilde{Z}_J(\omega_q), \quad (67)$$

which shows the suppression of the radiative decay induced by an underdamped JTL satisfying  $\alpha \ll 1$  (See Appendix C3). For concrete values of parameters in Table I, we estimate as  $\gamma(\omega_q) \simeq 87$  mHz for  $\alpha = 1.0 \times 10^{-5}$ . This is negligibly small in typical situations despite a finite amount of dissipation induced by intrinsic shunt resistors.

## VI. DISCUSSION

We observed that the time delay is proportional to the characteristic impedance  $Z_J$  of the JTL, and thus a high-impedance JTL is desirable for a readout with high accuracy. One promising approach is the use of high-kinetic-inductance material for the JTL [72], such as granular Al or NbN thin films [87, 88], to enlarge the quantumness  $Z_J/R_Q$  measured by the resistance quantum  $R_Q = h/(2e)^2$ . However, as the ratio  $Z_J/R_Q$  increases, quantum fluctuations of the fluxon become significant, and we cannot ignore its quantum nature any more and have to treat it as a quantum particle [69–71]. In such quantum regime of fluxon, we cannot rely on the classical treatment of the fluxon, which constitutes the basis of the present paper. Hence, one intriguing direction to be investigated is a fully quantum mechanical treatment of the time delay readout, which we leave for future work. Beyond the quantum regime, for  $Z_J/R_Q \simeq 1$  or further, which we might call deep quantum regime of fluxon, the quantum fluctuations become dominant and the picture of stable fluxon shall be violated [59, 70–72, 89]. This is another interesting system

to be investigated, whereas its utility as a readout probe would be limited.

Comparing our result with that for the time-delay readout of a flux qubit based on the inductive coupling [55], the feature of the absence of fluxon pinning for the capacitive coupling takes an advantage when slowing the fluxon to obtain a sufficiently large time delay. On the other hand, our scaling of the time delay  $1/u_0$  in the limit  $u_0 \rightarrow 0$  is milder compared with that  $1/u_0^3$  for inductive coupling, which could be in turn the disadvantage of our scheme. More quantitatively, the time delay of the fluxon induced by a flux qubit inductively coupled to a JTL reads  $\tau_{d,\text{FQ}} \simeq \phi_{\text{FQ}}/u_0^3$ , where  $\phi_{\text{FQ}}$  denotes the dimensionless coupling constant of the inductive coupling between the flux qubit and the JTL [55]. The pinning velocity  $u_{\text{pin}}$  below which the fluxon is pinned is  $u_{\text{pin}} := \sqrt{\phi_{\text{FQ}}/2}$  [55, 68]. In order to enhance the time delay without suffering from the pinning, we can not only decrease the initial velocity of the fluxon  $u_0$  but also adaptively change the coupling constant  $\phi_{\text{FQ}}$ , as  $\phi_{\text{FQ}} \propto u_0^2$ . Then, the inequality  $u_0 > u_{\text{pin}}$  is always satisfied even for a slower velocity  $u_0$  and the pinning can be avoided. Meanwhile, the scaling of the time delay becomes milder, as  $\tau_{\text{FQ}} \propto 1/u_0$ . This result shows that the scaling of the time delay  $\tau_d \propto 1/u_0$  is common for the capacitive and inductive coupling, under the condition of the absence of fluxon pinning.

## VII. CONCLUSION

We studied the time-delay readout of a superconducting qubit coupled with a JTL that serves not only as a transmission line for a propagating fluxon but also as a filter suppressing the radiative decay of the qubit. We concretely treat a transmon qubit under the two-level approximation capacitively coupled with a JTL and obtain analytical and numerical results of the time delay in good agreement, and the value of the time delay of a sufficiently slow fluxon in an underdamped JTL exceeds the typical time resolution of a time-delay detector based on SFQ digital circuits. Unlike the system of a flux qubit inductively coupled with a JTL [55], the fluxon pinning is absent for the capacitive coupling, which is advantageous for the time-delay readout. Nonadiabatic transitions caused by the fluxon are suppressed by slowing the fluxon initial velocity, and thus the use of a sufficiently slow fluxon enables the non-demolition and high-fidelity readout. We also generalize the framework to readout of a multi-level transmon without the two-level approximation, while the discrepancy between the analytical results of the time delay with and without the two-level approximation is probably due to virtual excitations to higher excited states. To evaluate the radiative decay rate of the qubit induced by the JTL possessing no fluxon, we approximate JJs in the JTL by linear inductors to describe small-amplitude oscillations around the minima of cosine potentials, after which we call the JTL a KGTL.

Then, due to the spectral gap of the KGTL, we obtain an exponentially suppressed decay rate as a function of distance from an external environment. Even for a dissipative JTL having normal current leakage induced by a finite subgap resistance, the leading-order contribution to the decay rate is proportional to the damping coefficient  $\alpha$  of the JTL, and it is also strongly suppressed for an underdamped JTL. Our readout scheme enables us to circumvent the wiring complexity and thermal-loaded overheads involved in the brute-force scaling of superconducting circuits with current technology, and it therefore opens the way towards a large-scale quantum computer with heterogeneous quantum-classical architecture based on the use of the SFQ digital logic family.

## ACKNOWLEDGMENTS

We thank Yoshihito Hashimoto and Ryoji Miyazaki for their insightful feedback. This work was supported by JST Moonshot R&D Grant Number JPMJMS2067, Japan.

### Appendix A: Effective Hamiltonian of transmon weakly coupled to JTL

#### 1. Schrieffer–Wolff (SW) transformation

We begin with the total Hamiltonian  $\hat{H}(t) := \hat{H}_0 + \hat{V}(t)$  composed of an easily diagonalizable free Hamiltonian  $\hat{H}_0$  and a small time-dependent perturbation Hamiltonian  $\hat{V}(t)$ . For an application of the Schrieffer–Wolff (SW) transformation, we adopt a time-dependent unitary operator  $\hat{U}(t) := e^{-\hat{S}(t)}$  that is determined by an anti-Hermitian operator  $\hat{S}(t)$ . Moving onto the rotating frame with respect to  $\hat{U}$ , a quantum state is transformed as  $|\psi_U(t)\rangle := \hat{U}|\psi(t)\rangle$  and the transformed Hamiltonian  $\hat{H}_U(t)$  reads

$$\hat{H}_U(t) := i\hbar \frac{\partial \hat{U}}{\partial t} \hat{U}^\dagger + \hat{U} \hat{H} \hat{U}^\dagger. \quad (\text{A1})$$

In terms of the anti-Hermitian operator  $\hat{S}(t)$ ,

$$\begin{aligned} \hat{H}_U = & -i\hbar \frac{\partial \hat{S}}{\partial t} + \hat{H}_0 + \hat{V} - [\hat{S}, \hat{H}_0] \\ & - [\hat{S}, \hat{V}] + \frac{1}{2} [\hat{S}, [\hat{S}, \hat{H}_0]] + \frac{1}{2} [\hat{S}, [\hat{S}, \hat{V}]] + \dots, \end{aligned} \quad (\text{A2})$$

which is derived from the Baker–Campbell–Hausdorff formula. Then, we impose the condition on  $\hat{S}$  that

$$\hat{V} = [\hat{S}, \hat{H}_0], \quad (\text{A3})$$

which gives us the unitary transformation called the SW transformation. Observing that  $\hat{S}$  is the same order as  $\hat{V}$  due to the above condition in Eq. (A3), we arrange the

transformed Hamiltonian  $\hat{H}_{\text{SW}}(t) := \hat{H}_U(t)$  with respect to the order of  $\hat{V}$  and obtain

$$\hat{H}_{\text{SW}} = -i\hbar \frac{\partial \hat{S}}{\partial t} + \hat{H}_0 - \frac{1}{2}[\hat{S}, \hat{V}] + O(\hat{V}^3). \quad (\text{A4})$$

Neglecting the higher-order terms  $O(\hat{V}^3)$  for a small perturbation Hamiltonian  $\hat{V}$ , we obtain the effective Hamiltonian

$$\hat{H}_{\text{SW}} \simeq -i\hbar \frac{\partial \hat{S}}{\partial t} + \hat{H}_0 - \frac{1}{2}[\hat{S}, \hat{V}]. \quad (\text{A5})$$

In general, we can diagonalize the free Hamiltonian as  $\hat{H}_0 = \sum_n \epsilon_n |\psi_n\rangle\langle\psi_n|$ . Then, the following anti-Hermitian operator  $\hat{S}(t)$  satisfies the condition of the SW transformation in Eq. (A3):

$$\hat{S}(t) := \sum_{n,m;\epsilon_n \neq \epsilon_m} \frac{\langle\psi_m|\hat{V}(t)|\psi_n\rangle}{\epsilon_n - \epsilon_m} |\psi_m\rangle\langle\psi_n|. \quad (\text{A6})$$

## 2. Two-level approximation

Under the two-level approximation,

$$\hat{H}_0 = \frac{\hbar\omega_q}{2} \hat{\sigma}_z, \quad (\text{A7})$$

$$\hat{V}(t) = \hbar g_c(t) \hat{\sigma}_y. \quad (\text{A8})$$

The SW transformation  $\hat{U}_{\text{SW}}(t) := e^{-\hat{S}(t)}$  is given by  $\hat{S}(t) := i(g_c(t)/\omega_q) \hat{\sigma}_x$  that leaves us the transformed Hamiltonian:

$$\hat{H}_{\text{SW}}(t) = \frac{\hbar\dot{g}_c(t)}{\omega_q} \hat{\sigma}_x + \frac{\hbar\omega_q}{2} \hat{\sigma}_z + \frac{\hbar g_c^2(t)}{\omega_q} \hat{\sigma}_z + O(g_c^3). \quad (\text{A9})$$

We obtain the effective Hamiltonian in Eq. (24) in the main text by neglecting the higher-order terms  $O(g_c^3)$  and the first term in the right-hand side proportional to the time derivative  $\dot{g}_c(t)$ , which is validated for a weak coupling a small fluxon velocity satisfying  $u_0 \ll \omega_q/\omega_p$ . Although one might worry about the difference of the frame before and after the SW transformation, the coupling amplitude  $g_c(t)$  is zero after the fluxon scattering, and thus we go back to the original frame.

## 3. Multi-level transmon

For a multi-level transmon, the Hamiltonians are

$$\hat{H}_0 := \sum_n E_n |n\rangle\langle n|, \quad (\text{A10})$$

$$\hat{V}(t) := -i\sqrt{2}\mathcal{E}(\hat{a} - \hat{a}^\dagger), \quad (\text{A11})$$

where  $\mathcal{E} := en_{0,\text{tr}} C_c Q_m / (C_\Sigma C_J)$ . The SW-transformed Hamiltonian is  $\hat{H}_{\text{SW}} = \hat{H}_0 + (\hat{V}\hat{S} + \text{H.c.})/2$ , where

$$\frac{1}{2\mathcal{E}^2} \hat{V}\hat{S} = (\hat{a} - \hat{a}^\dagger) \sum_{n,m} \frac{\langle m|(\hat{a} - \hat{a}^\dagger)|n\rangle}{E_m - E_n} |m\rangle\langle n|. \quad (\text{A12})$$

The symbol ‘‘H.c.’’ denotes the Hermitian conjugate. After some calculations, we obtain  $\frac{1}{2}\hat{V}\hat{S} + \text{H.c.} = \hat{D} + \hat{W}$ , where

$$\hat{D} := -\frac{2\mathcal{E}^2}{\hbar\omega_{\text{tr}}} \sum_{n=0}^{\infty} \frac{1}{[1-np][1-(n+1)p]} |n\rangle\langle n|, \quad (\text{A13})$$

$$\begin{aligned} \hat{W} := & -\frac{p\mathcal{E}^2}{\hbar\omega_{\text{tr}}} \sum_{n=0}^{\infty} \frac{\sqrt{(n+1)(n+2)}}{[1-(n+1)p][1-(n+2)p]} |n+2\rangle\langle n| \\ & + \text{H.c.} \end{aligned} \quad (\text{A14})$$

To safely neglect the off-diagonal term  $\hat{W}$ , we impose the condition on the photon number  $n$  of interest, that

$$\frac{1-(n+2)p}{p(1-np)} \gg \frac{1}{2} \sqrt{(n+1)(n+2)}. \quad (\text{A15})$$

For  $p = 1/20$ , the ratio  $Q(n) := L(n)/R(n)$  of the left-hand side  $L(n) := \frac{1-(n+2)p}{p(1-np)}$  to the right-hand side  $R(n) := \frac{1}{2} \sqrt{(n+1)(n+2)}$  satisfies  $Q(n) \geq 10$  for  $n = 0, 1, 2$ , which validates the effective Hamiltonian in Eq. (51) up to  $n = 2$ . A smaller  $p$  validates the effective Hamiltonian for a larger photon number  $n$ , while the time delay is proportional to  $p$  and thus unfavorably decreases. Neglecting the off-diagonal term  $\hat{W}$ , we obtain  $\hat{H}_{\text{SW}} \simeq \hat{H}_0 + \hat{D}$  and recover the SW-transformed Hamiltonian in Eq. (51) in the main text.

## Appendix B: Perturbation theory of sine-Gordon kink

### 1. Perturbation term for a transmon qubit under the two-level approximation

We recall the perturbed JTL Hamiltonian in Eq. (26) in the main text. The perturbation term can be attributed to the change in the capacitance of the  $m$ -th junction of JTL  $C_J \mapsto C_J + \delta C_J(\sigma_z)$ , where  $\delta C_J(\sigma_z)$  depends on the state of qubit as

$$\delta C_J(\sigma_z) := -4n_{0,\text{tr}}^2 \frac{e^2}{\hbar\omega_q} \frac{C_c^2}{C_\Sigma^2} \sigma_z. \quad (\text{B1})$$

We neglected higher-order terms  $O(C_c^4)$ . Remembering the discretized sine-Gordon equation in Eq. (2) in the main text, the perturbed fluxon obeys the following equation:

$$\begin{aligned} & \frac{\varphi_0 C_J}{I_c} \frac{\partial^2 \phi_n}{\partial t^2} - \frac{\varphi_0}{L I_c} (\phi_{n+1} - 2\phi_n + \phi_{n-1}) + \sin \phi_n \\ & = -\delta_{n,m} \frac{\varphi_0}{I_c} \delta C_J(\sigma_z) \frac{\partial^2 \phi_n}{\partial t^2}. \end{aligned} \quad (\text{B2})$$

In the continuum limit, the last term in the right-hand side can be arranged, as

$$\begin{aligned} & -\delta_{n,m} \frac{\varphi_0}{I_c} \delta C_J(\sigma_z) \frac{\partial^2 \phi_n}{\partial t^2} \\ & = \frac{\delta_{n,m} \varphi_0}{\Delta x i_c} \cdot 4n_{0,\text{tr}}^2 \frac{e^2}{\hbar \omega_q} \frac{C_c^2}{C_\Sigma^2} \sigma_z \frac{\partial^2 \phi_n}{\partial t^2} \\ & \rightarrow \delta(\xi) \frac{\varphi_0}{\lambda_J i_c} \cdot 4n_{0,\text{tr}}^2 \frac{e^2}{\hbar \omega_q} \frac{C_c^2}{C_\Sigma^2} \omega_p^2 \sigma_z \frac{\partial^2 \phi_n}{\partial \tau^2}, \end{aligned} \quad (\text{B3})$$

where we used the correspondence  $\delta_{n,m}/\Delta x \rightarrow \delta(x) = \lambda_J^{-1} \delta(\xi)$  and  $\partial_t = \omega_p \partial_\tau$ . Finally, noticing

$$\frac{\varphi_0}{\lambda_J i_c} \frac{4n_{0,\text{tr}}^2 e^2}{\hbar \omega_q} \frac{C_c^2}{C_\Sigma^2} \omega_p^2 = \frac{C_c^2 / (\lambda_J c_J C_\Sigma)}{1 - \sqrt{E_{C,\text{tr}} / (8E_{J,\text{tr}})}}, \quad (\text{B4})$$

we reproduce the perturbed sine-Gordon equation in Eq. (27) in the main text.

## 2. Perturbation term for a multilevel transmon

For a multi-level transmon, the change in the capacitance of the  $m$ -th junction of the JTTL is given by Eq. (52). We then derive the perturbation term for the sine-Gordon equation, as

$$\begin{aligned} & -\delta_{k,m} \frac{\varphi_0}{I_c} \frac{C_c^2 / C_\Sigma}{[1-np][1-(n+1)p]} \frac{\partial^2 \phi_k}{\partial t^2} \\ & \rightarrow \frac{-1}{[1-np][1-(n+1)p]} \frac{C_c^2}{\lambda_J c_J C_\Sigma} \delta(\xi) \partial_\tau^2 \phi, \end{aligned} \quad (\text{B5})$$

which gives us the dimensionless constant  $\eta_{c,\text{tr}} = \eta_{c,\text{mlt}}(|n|)$  in Eq. (53).

## 3. Differential equations for $u(\tau)$ and $\Xi(\tau)$

According to the perturbation theory of sine-Gordon kinks provided in Refs. [66, 67], we begin with the following sine-Gordon equation with a perturbation term  $f(\phi, \xi)$ :

$$\partial_\tau^2 \phi - \partial_\xi^2 \phi + \sin \phi = \gamma - \alpha \partial_\tau \phi + f(\phi, \xi). \quad (\text{B6})$$

The perturbation theory is based on the assumptions that  $|\gamma|, \alpha, |f| \ll 1$  under which the soliton shape is preserved and the perturbed solution of the dimensionless modulated velocity  $u(\tau)$  and the centroid  $\Xi(\tau)$  in Eq. (9) well approximates the true solution. Then, for a perturbation term  $f(\phi, \xi)$ , the modulation parameters  $u(\tau)$  and  $\Xi(\tau)$  obey the following ordinary differential equations [55, 66, 67]:

$$\begin{aligned} \frac{du}{d\tau} & = -\frac{1}{4} \pi \gamma (1-u^2)^{\frac{3}{2}} - \alpha u (1-u^2) \\ & \quad - \frac{1}{4} (1-u^2) \int_{-\infty}^{\infty} d\xi f(\phi(\xi, \tau), \xi) \text{sech} \Theta, \end{aligned} \quad (\text{B7})$$

$$\frac{d\Xi}{d\tau} = u - \frac{1}{4} u \sqrt{1-u^2} \int_{-\infty}^{\infty} d\xi f(\phi(\xi, \tau), \xi) \Theta \text{sech} \Theta, \quad (\text{B8})$$

where we define the function  $\Theta = \Theta(\xi, \tau)$  as

$$\Theta(\xi, \tau) := \frac{\xi - \Xi(\tau)}{\sqrt{1-u^2(\tau)}}. \quad (\text{B9})$$

For a JTTL capacitively coupled to a transmon, the perturbation term takes the form

$$f(\phi, \xi) = \eta_{c,\text{tr}} \delta(\xi) \partial_\tau^2 \phi(\xi, \tau), \quad (\text{B10})$$

which is applicable both for transmons with and without the two-level approximation. The dimensionless constant  $\eta_{c,\text{tr}}$  such that  $|\eta_{c,\text{tr}}| \ll 1$  depends on the quantum state of the transmon. The perturbation term can be expanded as

$$f(\phi, \xi) = \eta_{c,\text{tr}} \delta(\xi) \partial_\tau^2 (4 \arctan [e^\Theta]) \quad (\text{B11})$$

$$\begin{aligned} & = -\eta_{c,\text{tr}} \delta(\xi) \frac{2u^2(\tau)}{1-u^2(\tau)} \text{sech}^2(\Theta) \sinh(\Theta) \\ & \quad + O(\eta_{c,\text{tr}}^2), \end{aligned} \quad (\text{B12})$$

where we assume the expansion  $u(\tau) = u_0 + O(\eta_{c,\text{tr}})$  around the unperturbed initial velocity  $u_0$  and neglect the higher order terms  $O(\eta_{c,\text{tr}}^2)$ . Putting this result into Eqs. (B7) and (B8) and executing the integral, we obtain

$$\begin{aligned} \frac{du}{d\tau} & = -\frac{1}{4} \pi \gamma (1-u^2)^{\frac{3}{2}} - \alpha u (1-u^2) \\ & \quad - \frac{1}{2} \eta_{c,\text{tr}} u^2 \text{sech}^3(\Theta_0) \sinh(\Theta_0), \end{aligned} \quad (\text{B13})$$

$$\frac{d\Xi}{d\tau} = u + \frac{1}{2} \eta_{c,\text{tr}} \frac{u^3}{\sqrt{1-u^2}} \Theta_0 \text{sech}^3(\Theta_0) \sinh(\Theta_0). \quad (\text{B14})$$

Here, we introduce the time-dependent function  $\Theta_0 := -\Theta(0, \tau) = \Xi(\tau) / \sqrt{1-u^2(\tau)}$ , which also appears in the main text.

## 4. Analytical solution of $u(\tau)$ for capacitive coupling

To obtain analytical results, we assume the following conditions:

$$|\gamma| \ll |\eta_{c,\text{tr}}| u^2, \quad (\text{B15})$$

$$\alpha \ll |\eta_{c,\text{tr}}| u. \quad (\text{B16})$$

In this case, the equation for the modulation parameter  $u(\tau)$  is simplified as

$$\frac{du}{d\tau} = -\frac{1}{2} \eta_{c,\text{tr}} u^2 \text{sech}^3(\Theta_0) \sinh(\Theta_0). \quad (\text{B17})$$

We set the ansatz

$$\sqrt{1-u^2} = \sqrt{1-u_0^2} \left[ 1 + \frac{1}{2} \eta_{c,\text{tr}} F(\Theta_0) \right]. \quad (\text{B18})$$

This is based on the observation that the velocity is  $u_0$  in the absence of transmon (i.e.  $\eta_{c,\text{tr}} = 0$ ), and we are now

interested in the case  $|\eta_{c,\text{tr}}| \ll 1$  and thus the higher-order terms are negligible. Taking time derivative of the both sides in Eq. (B18) and noticing the equation

$$(\partial_\tau \Xi) \sqrt{1-u^2} + \frac{u\Xi}{\sqrt{1-u^2}} \partial_\tau u = u \sqrt{1-u^2}, \quad (\text{B19})$$

we obtain the following equation for the function  $F$ :

$$\frac{dF}{d\Theta_0} = \frac{u_0^2}{\sqrt{1-u_0^2}} \text{sech}^3(\Theta_0) \sinh(\Theta_0) + O(\eta_{c,\text{tr}}). \quad (\text{B20})$$

We find the analytical solution of the velocity  $u(\tau)$ , which satisfies Eqs. (B14) and (B17) under the ignorance of higher-order terms  $O(\eta_{c,\text{tr}}^2)$ :

$$\sqrt{1-u^2} = \sqrt{1-u_0^2} \left[ 1 - \frac{1}{4} \eta_{c,\text{tr}} \frac{u_0^2}{\sqrt{1-u_0^2}} \text{sech}^2(\Theta_0) \right]. \quad (\text{B21})$$

Especially for  $\eta_{c,\text{tr}} = \eta_c \sigma_z$ , this result recovers Eq. (33) under the two-level approximation in the main text. This result also corresponds to the results in Eqs. (24) and (33) in Ref. [55] derived for flux qubits, while the prefactors and function forms are distinct. We can also recover analytical expressions of time delay for multi-level transmon from this result, by choosing  $\eta_{c,\text{tr}} = \eta_{c,\text{mlt}}(|n\rangle)$  in Eq. (53) in the main text. We did not assume any condition for the initial velocity  $u_0$ , thus the expression in Eq. (B21) is applicable for an arbitrarily chosen initial velocity  $u_0$  of the fluxon, while only slow fluxons are considered for analytical expressions in Ref. [55].

## Appendix C: Radiative decay induced by KGTL

### 1. Admittance and radiative decay rate

We here derive the admittance of a KGTL seen by a capacitively coupled transmon at one end, and the other end is terminated by an external source (See Fig. 5 (a) and (b)).

We set the coordinate  $x$  along the KGTL, whose terminated end is at  $x = 0$  and the other coupled to the transmon is at  $x = l/2$ , thus the length of KGTL is  $l/2$ . We assume that  $Z(x)$  denotes the impedance of the KGTL of length  $x$  seen from the end to the ground. We write down the recurrence relation of the impedance  $Z(x + \Delta x)$  for the next KGTL to which we added one unit cell at  $x + \Delta x$ :

$$Z(x + \Delta x) = i\omega L + \left[ \frac{1}{Z(x)} + G_J + \frac{1}{i\omega L_J} + i\omega C_J \right]^{-1}. \quad (\text{C1})$$

In the continuum limit, we neglect the higher-order terms  $O(\Delta x^2)$  and assume  $\{Z(x + \Delta x) - Z(x)\}/\Delta x \simeq$

$dZ/dx$ . We then obtain the following differential equation of  $Z(x)$ :

$$\frac{dZ}{dx} + X_0 Z^2 = i\omega \ell, \quad (\text{C2})$$

where

$$X_0 := g_J - i\omega C_J \left( \frac{\omega_p^2}{\omega^2} - 1 \right). \quad (\text{C3})$$

The definitions of parameters in the continuum limit are presented in the main text. This is a type of differential equation called Riccati's equation, and we can analytically solve it:

$$Z(x) = \lambda_0 \frac{(Z_0 + \lambda_0)e^{\lambda_0 X_0 x} + (Z_0 - \lambda_0)e^{-\lambda_0 X_0 x}}{(Z_0 + \lambda_0)e^{\lambda_0 X_0 x} - (Z_0 - \lambda_0)e^{-\lambda_0 X_0 x}}, \quad (\text{C4})$$

where we introduced a complex parameter  $\lambda_0 := \sqrt{i\omega \ell / X_0}$ . Another parameter  $Z_0 := R_{\text{in}} + i\omega L_{\text{in}}$  denotes the external impedance and gives the boundary condition  $Z(0) = Z_0$ .

The transmon qubit is coupled to the KGTL via the capacitor  $C_c$ , and the KGTL is terminated by the external source  $Z_0$  at  $x = 0$ . Then, effective impedance  $Z_{\text{eff}}$  that the transmon sees reads

$$Z_{\text{eff}}(\omega) := Z_1(l/2) + i \left[ Z_2(l/2) - \frac{1}{\omega C_c} \right], \quad (\text{C5})$$

where  $Z_1(x) := \text{Re}[Z(x)]$  and  $Z_2(x) := \text{Im}[Z(x)]$ . Evaluating the effective admittance  $Y(\omega) := Z_{\text{eff}}^{-1}(\omega)$ , we can estimate the radiative decay rate  $\gamma(\omega_q)$  at the transmon angular frequency  $\omega = \omega_q$  induced by the externally terminated KGTL [90, 91]:

$$\begin{aligned} \gamma(\omega_q) &:= \frac{1}{C_\Sigma} \text{Re}[Y(\omega_q)] \\ &= \frac{1}{C_\Sigma} \frac{Z_1(l/2)}{Z_1^2(l/2) + [Z_2(l/2) - 1/(\omega C_c)]^2} \Big|_{\omega=\omega_q}. \end{aligned} \quad (\text{C6})$$

### 2. Decay rate for dissipationless KGTL

For a dissipationless KGTL, i.e.  $g_J = 0$ , then

$$\lambda_0 X_0 = \frac{1}{\lambda_J} \frac{\omega}{\omega_p} \sqrt{\frac{\omega_p^2}{\omega^2} - 1}. \quad (\text{C7})$$

The transmon angular frequency  $\omega = \omega_q \simeq 2\pi \times 3.7$  GHz and the JTL plasma frequency  $\omega_p \simeq 360$  GHz are typical values, and then  $\omega \ll \omega_p$  and  $\lambda_0 X_0 \simeq 1/\lambda_J$ . As a result, we can approximate the impedance  $Z(x)$ , as

$$Z(l/2) = \lambda_0 + 2\lambda_0 \frac{Z_0^2 - \lambda_0^2}{(Z_0 + \lambda_0)^2} \Gamma_0 + O(\Gamma_0^2), \quad (\text{C8})$$

where  $\Gamma_0 := e^{-\lambda_0 X_0 l}$  is an exponentially decaying function with respect to the length  $l/2$  of KGTL. Under the

present conditions,  $\lambda_0 = i\tilde{Z}_J$  is pure imaginary and thus the real and imaginary parts  $Z_1(x)$  and  $Z_2(x)$  respectively read

$$Z_1(x) = 2\text{Re} \left[ i\tilde{Z}_J \frac{Z_0^2 + \tilde{Z}_J^2}{(Z_0 + i\tilde{Z}_J)^2} \right] \Gamma_0 + O(\Gamma_0^2), \quad (\text{C9})$$

$$Z_2(x) = \tilde{Z}_J + O(\Gamma_0), \quad (\text{C10})$$

where  $\tilde{Z}_J(\omega) := Z_J / \sqrt{(\omega_p^2/\omega^2) - 1}$ . The radiative decay rate in Eq. (C6) is then written as

$$\gamma(\omega_q) = \frac{2\text{Re} \left[ i\tilde{Z}_J \frac{(Z_0^2 + \tilde{Z}_J^2)}{(Z_0 + i\tilde{Z}_J)^2} \right]}{C_\Sigma \left[ \tilde{Z}_J - 1/(\omega C_c) \right]^2} \Gamma_0 \Big|_{\omega=\omega_q} + O(\Gamma_0^2), \quad (\text{C11})$$

which clearly manifests the exponential suppression of the radiative decay rate due to the factor  $\Gamma_0(\omega_q) \simeq e^{-l/\lambda_J}$ . This result yields Eq. (65) in the main text. To see an explicit expression, we assume that  $L_{\text{in}} = 0$ , then  $Z_0 = R_{\text{in}}$  and we obtain

$$\text{Re} \left[ i\tilde{Z}_J \frac{Z_0^2 + \tilde{Z}_J^2}{(Z_0 + i\tilde{Z}_J)^2} \right] = \frac{2R_{\text{in}}\tilde{Z}_J^2}{R_{\text{in}}^2 + \tilde{Z}_J^2}. \quad (\text{C12})$$

This leads us to a simple expression of the radiative decay rate:

$$\gamma(\omega_q) \simeq \frac{4}{C_\Sigma} \frac{1}{\left[ \tilde{Z}_J(\omega_q) - 1/(\omega_q C_c) \right]^2} \frac{R_{\text{in}}\tilde{Z}_J^2(\omega_q)}{R_{\text{in}}^2 + \tilde{Z}_J^2(\omega_q)} \Gamma_0(\omega_q). \quad (\text{C13})$$

We furthermore consider the situation in which  $1/(\omega_q C_c) \gg \tilde{Z}_J(\omega_q)$ , then

$$\gamma(\omega_q) \simeq 4\omega_q^2 \frac{C_c^2}{C_\Sigma} \frac{R_{\text{in}}\tilde{Z}_J^2(\omega_q)}{R_{\text{in}}^2 + \tilde{Z}_J^2(\omega_q)} \Gamma_0(\omega_q), \quad (\text{C14})$$

which reproduces Eq. (66) in the main text under the additional assumption for a low-impedance JTL  $\tilde{Z}_J(\omega_q) \ll R_{\text{in}}$ .

### 3. Decay rate for dissipative KGTL

We here address the radiative decay induced by a dissipative KGTL, in which a finite amount of dissipation occurs. In this case, the exponent in the impedance

$Z(x)$  reads

$$\begin{aligned} \lambda_0 X_0 &= \sqrt{i\omega \ell X_0} \\ &= \frac{\omega}{\lambda_J \omega_p} \sqrt{\frac{\omega_p^2}{\omega^2} - 1} \left[ 1 + i \frac{\alpha \omega_p / \omega}{(\omega_p^2 / \omega^2) - 1} \right]^{1/2}. \end{aligned} \quad (\text{C15})$$

We assume that  $\alpha \ll 1$  that is validated for an underdamped (but dissipative) JTL and  $\omega < \omega_p$ , then  $k_1 := \text{Re}[\lambda_0 X_0]$  and  $k_2 := \text{Im}[\lambda_0 X_0]$  are respectively approximated as

$$k_1 \simeq \frac{\omega}{\lambda_J \omega_p} \sqrt{\frac{\omega_p^2}{\omega^2} - 1}, \quad (\text{C16})$$

$$k_2 \simeq \frac{\alpha}{2\lambda_J} \frac{1}{\sqrt{(\omega_p^2 / \omega^2) - 1}}. \quad (\text{C17})$$

Going back to the expression of  $Z(l/2)$ ,

$$Z(l/2) = \lambda_0 \frac{(Z_0 + \lambda_0) + (Z_0 - \lambda_0)e^{-ik_2 l} \Gamma_1}{(Z_0 + \lambda_0) - (Z_0 - \lambda_0)e^{-ik_2 l} \Gamma_1}, \quad (\text{C18})$$

where  $\Gamma_1 := e^{-k_1 l}$ . Neglecting the exponentially small factor  $\Gamma_1$  for  $k_1 l \simeq l/\lambda_J \gg 1$ , we obtain

$$Z(l/2) \simeq \lambda_0. \quad (\text{C19})$$

We then estimate the real and imaginary parts of  $\lambda_0$ , as

$$\text{Re}[\lambda_0] = \frac{\alpha}{2} \frac{Z_J}{\sqrt{(\omega_p^2 / \omega^2) - 1}} \frac{\omega_p / \omega}{(\omega_p^2 / \omega^2) - 1} + O(\alpha^3), \quad (\text{C20})$$

$$\text{Im}[\lambda_0] = \frac{Z_J}{\sqrt{(\omega_p^2 / \omega^2) - 1}} \left[ 1 - \frac{\alpha^2}{2} \frac{\omega_p^2 / \omega^2}{[(\omega_p^2 / \omega^2) - 1]^2} \right], \quad (\text{C21})$$

which are justified under the present situation satisfying  $(\alpha \omega_p / \omega) / [(\omega_p^2 / \omega^2) - 1] \ll 1$ . Plugging  $Z_1 = \text{Re}[\lambda_0]$  and  $Z_2 = \text{Im}[\lambda_0]$  into Eq. (C6), we arrive at

$$\gamma(\omega_q) \simeq \frac{\alpha}{2} \frac{\tilde{Z}_J(\omega_q)}{C_\Sigma [\tilde{Z}_J(\omega_q) - 1/(\omega_q C_c)]^2} \frac{\omega_p / \omega_q}{(\omega_p^2 / \omega_q^2) - 1}, \quad (\text{C22})$$

where we neglect the higher-order terms  $O(\alpha^3)$ . Approximate it further using the relations  $\omega_q C_c \ll \tilde{Z}_J^{-1}(\omega_q)$  and  $\omega_p \gg \omega_q$ , we then end up with Eq. (67) in the main text.

[1] Y. Nakamura, Y. A. Pashkin, and J. Tsai, Coherent control of macroscopic quantum states in a single-cooper-pair box, *Nature* **398**, 786 (1999).

[2] J. Mooij, T. Orlando, L. Levitov, L. Tian, C. H. Van der Wal, and S. Lloyd, Josephson persistent-current qubit, *Science* **285**, 1036 (1999).

- [3] J. M. Martinis, S. Nam, J. Aumentado, and C. Urbina, Rabi oscillations in a large Josephson-junction qubit, *Phys. Rev. Lett.* **89**, 117901 (2002).
- [4] J. Koch, T. M. Yu, J. Gambetta, A. A. Houck, D. I. Schuster, J. Majer, A. Blais, M. H. Devoret, S. M. Girvin, and R. J. Schoelkopf, Charge-insensitive qubit design derived from the Cooper pair box, *Phys. Rev. A* **76**, 042319 (2007).
- [5] V. E. Manucharyan, J. Koch, L. I. Glazman, and M. H. Devoret, Fluxonium: Single Cooper-pair circuit free of charge offsets, *Science* **326**, 113 (2009).
- [6] Z. Leghtas, S. Touzard, I. M. Pop, A. Kou, B. Vlastakis, A. Petrenko, K. M. Sliwa, A. Narla, S. Shankar, M. J. Hatridge, *et al.*, Confining the state of light to a quantum manifold by engineered two-photon loss, *Science* **347**, 853 (2015).
- [7] P. W. Shor, Algorithms for quantum computation: discrete logarithms and factoring, in *Proceedings 35th annual symposium on foundations of computer science (IEEE, 1994)* pp. 124–134.
- [8] L. K. Grover, Quantum mechanics helps in searching for a needle in a haystack, *Phys. Rev. Lett.* **79**, 325 (1997).
- [9] M. A. Nielsen and I. L. Chuang, *Quantum computation and quantum information* (Cambridge university press, 2010).
- [10] P. W. Shor, Scheme for reducing decoherence in quantum computer memory, *Phys. Rev. A* **52**, R2493 (1995).
- [11] S. B. Bravyi and A. Y. Kitaev, Quantum codes on a lattice with boundary, arXiv: 9811052 (1998).
- [12] A. G. Fowler, M. Mariantoni, J. M. Martinis, and A. N. Cleland, Surface codes: Towards practical large-scale quantum computation, *Phys. Rev. A* **86**, 032324 (2012).
- [13] D. Horsman, A. G. Fowler, S. Devitt, and R. V. Meter, Surface code quantum computing by lattice surgery, *New J. Phys.* **14**, 123011 (2012).
- [14] R. McDermott, M. G. Vavilov, B. L. T. Plourde, F. K. Wilhelm, P. J. Liebermann, O. A. Mukhanov, and T. A. Ohki, Quantum-classical interface based on single flux quantum digital logic, *Quant. Sci. Technol.* **3**, 024004 (2018).
- [15] D. P. DiVincenzo, The physical implementation of quantum computation, *Fortschr. Phys.* **48**, 771 (2000).
- [16] Y. Y. Gao, M. A. Rol, S. Touzard, and C. Wang, Practical guide for building superconducting quantum devices, *PRX Quantum* **2**, 040202 (2021).
- [17] A. Blais, R.-S. Huang, A. Wallraff, S. M. Girvin, and R. J. Schoelkopf, Cavity quantum electrodynamics for superconducting electrical circuits: An architecture for quantum computation, *Phys. Rev. A* **69**, 062320 (2004).
- [18] A. Wallraff, D. I. Schuster, A. Blais, L. Frunzio, R.-S. Huang, J. Majer, S. Kumar, S. M. Girvin, and R. J. Schoelkopf, Strong coupling of a single photon to a superconducting qubit using circuit quantum electrodynamics, *Nature* **431**, 162 (2004).
- [19] D. Schuster, A. A. Houck, J. Schreier, A. Wallraff, J. Gambetta, A. Blais, L. Frunzio, J. Majer, B. Johnson, M. Devoret, *et al.*, Resolving photon number states in a superconducting circuit, *Nature* **445**, 515 (2007).
- [20] E. M. Purcell, Spontaneous emission probabilities at radio frequencies, *Phys. Rev.* **69**, 681 (1946).
- [21] U. Fano, Effects of configuration interaction on intensities and phase shifts, *Phys. Rev.* **124**, 1866 (1961).
- [22] C. W. Gardiner and M. J. Collett, Input and output in damped quantum systems: Quantum stochastic differential equations and the master equation, *Phys. Rev. A* **31**, 3761 (1985).
- [23] G. Burkard, R. H. Koch, and D. P. DiVincenzo, Multi-level quantum description of decoherence in superconducting qubits, *Phys. Rev. B* **69**, 064503 (2004).
- [24] K. Koshino and A. Shimizu, Quantum zeno effect by general measurements, *Physics Reports* **412**, 191 (2005).
- [25] A. A. Houck, J. Schreier, B. Johnson, J. Chow, J. Koch, J. Gambetta, D. Schuster, L. Frunzio, M. Devoret, S. Girvin, *et al.*, Controlling the spontaneous emission of a superconducting transmon qubit, *Phys. Rev. Lett.* **101**, 080502 (2008).
- [26] E. Jeffrey, D. Sank, J. Mutus, T. White, J. Kelly, R. Barends, Y. Chen, Z. Chen, B. Chiaro, A. Dunsworth, *et al.*, Fast accurate state measurement with superconducting qubits, *Phys. Rev. Lett.* **112**, 190504 (2014).
- [27] E. A. Sete, J. M. Martinis, and A. N. Korotkov, Quantum theory of a bandpass Purcell filter for qubit readout, *Phys. Rev. A* **92**, 012325 (2015).
- [28] A. Blais, A. L. Grimsmo, S. M. Girvin, and A. Wallraff, Circuit quantum electrodynamics, *Rev. Mod. Phys.* **93**, 025005 (2021).
- [29] T. Thorbeck, Z. Xiao, A. Kamal, and L. C. Govia, Readout-induced suppression and enhancement of superconducting qubit lifetimes, *Phys. Rev. Lett.* **132**, 090602 (2024).
- [30] A. Bengtsson, A. Opremcak, M. Khezri, D. Sank, A. Bourassa, K. J. Satzinger, S. Hong, C. Erickson, B. J. Lester, K. C. Miao, *et al.*, Model-based optimization of superconducting qubit readout, *Phys. Rev. Lett.* **132**, 100603 (2024).
- [31] D. Sank, Z. Chen, M. Khezri, J. Kelly, R. Barends, B. Campbell, Y. Chen, B. Chiaro, A. Dunsworth, A. Fowler, *et al.*, Measurement-induced state transitions in a superconducting qubit: Beyond the rotating wave approximation, *Phys. Rev. Lett.* **117**, 190503 (2016).
- [32] R. Shillito, A. Petrescu, J. Cohen, J. Beall, M. Hauru, M. Ganahl, A. G. Lewis, G. Vidal, and A. Blais, Dynamics of transmon ionization, *Phys. Rev. Applied* **18**, 034031 (2022).
- [33] M. Khezri, A. Opremcak, Z. Chen, K. C. Miao, M. McEwen, A. Bengtsson, T. White, O. Naaman, D. Sank, A. N. Korotkov, *et al.*, Measurement-induced state transitions in a superconducting qubit: Within the rotating-wave approximation, *Phys. Rev. Applied* **20**, 054008 (2023).
- [34] M. F. Dumas, B. Groleau-Paré, A. McDonald, M. H. Muñoz-Arias, C. Lledó, B. D’Anjou, and A. Blais, Measurement-induced transmon ionization, *Phys. Rev. X* **14**, 041023 (2024).
- [35] K. N. Nesterov and I. V. Pechenezhskiy, Measurement-induced state transitions in dispersive qubit readout schemes, *Phys. Rev. Applied* **22**, 064038 (2024).
- [36] Y. Ye, J. B. Kline, S. Chen, A. Yen, and K. P. O’Brien, Ultrafast superconducting qubit readout with the quarton coupler, *Science Advances* **10**, eado9094 (2024).
- [37] M. Féchant, M. F. Dumas, D. Bénâtre, N. Gosling, P. Lenhard, M. Specker, S. Geisert, S. Ihssen, W. Wernsdorfer, B. D’Anjou, *et al.*, Offset charge dependence of measurement-induced transitions in transmons, *Phys. Rev. Lett.* **135**, 180603 (2025).

- [38] S. Singh, G. Refael, A. Clerk, and E. Rosenfeld, Impact of josephson-junction array modes on fluxonium readout, *PRX Quantum* **6**, 040304 (2025).
- [39] K. K. Likharev and V. K. Semenov, RSFQ logic/memory family: A new josephson-junction technology for sub-terahertz-clock-frequency digital systems, *IEEE Trans. Appl. Supercond.* **1**, 3 (1991).
- [40] D. Kirichenko, S. Sarwana, and A. Kirichenko, Zero static power dissipation biasing of RSFQ circuits, *IEEE Trans. Appl. Supercond.* **21**, 776 (2011).
- [41] N. Takeuchi, D. Ozawa, Y. Yamanashi, and N. Yoshikawa, An adiabatic quantum flux parametron as an ultra-low-power logic device, *Supercond. Sci. Technol.* **26**, 035010 (2013).
- [42] M. Mohseni, A. Scherer, K. G. Johnson, O. Wertheim, M. Otten, N. A. Aadit, Y. Alexeev, K. M. Bresniker, K. Y. Camsari, B. Chapman, *et al.*, How to build a quantum supercomputer: Scaling from hundreds to millions of qubits, arXiv:2411.10406 (2024).
- [43] J. Bernhardt, C. Jordan, J. Rahamim, A. Kirichenko, K. Bharadwaj, L. Fry-Bouriaux, K. Porsch, A. Somoroff, K.-T. Tsai, J. Walter, *et al.*, Quantum computer controlled by superconducting digital electronics at millikelvin temperature, arXiv:2503.09879 (2025).
- [44] J. Walter, A. C. Weis, K.-T. Tsai, M.-J. Yu, N. Katam, A. F. Kirichenko, O. A. Mukhanov, S.-J. Han, and I. V. Vernik, Single flux quantum circuit operation at millikelvin temperatures, *IEEE Trans. Appl. Supercond.* **36**, 1 (2025).
- [45] S. Kawabata, Integration and resource estimation of cryoelectronics for superconducting fault-tolerant quantum computers, arXiv:2601.03922 (2026).
- [46] R. McDermott and M. Vavilov, Accurate qubit control with single flux quantum pulses, *Phys. Rev. Applied* **2**, 014007 (2014).
- [47] Y. Wang, W. Gao, K. Liu, B. Ji, Z. Wang, and Z. Lin, Single-flux-quantum-activated controlled-z gate for transmon qubits, *Phys. Rev. Applied* **19**, 044031 (2023).
- [48] H. G. Tonchev, B. T. Torosov, and N. V. Vitanov, Robust, fast, and high-fidelity composite single-qubit gates for superconducting transmon qubits, *Phys. Rev. A* **112**, 012605 (2025).
- [49] B. Torosov, B. Kulchytskyy, F. Hopfmueller, J. Gundersen, X. Kong, and P. Ronagh, Optimization of two-qubit gates in tunable-coupler architectures using single-flux-quantum control, *Phys. Rev. A* **112**, 032613 (2025).
- [50] M. Lapointe-Major, B. Torosov, B. Kulchytskyy, and P. Ronagh, Optimization of high-fidelity single-qubit gates for fluxoniums using single-flux quantum control, arXiv:2511.14746 (2025).
- [51] E. Leonard Jr, M. A. Beck, J. Nelson, B. G. Christensen, T. Thorbeck, C. Howington, A. Opremcak, I. V. Pechenezhskiy, K. Dodge, N. P. Dupuis, *et al.*, Digital coherent control of a superconducting qubit, *Phys. Rev. Applied* **11**, 014009 (2019).
- [52] C.-H. Liu, A. Ballard, D. Olaya, D. R. Schmidt, J. Biesecker, T. Lucas, J. Ullom, S. Patel, O. Rafferty, A. Opremcak, *et al.*, Single flux quantum-based digital control of superconducting qubits in a multichip module, *PRX Quantum* **4**, 030310 (2023).
- [53] K. Liu, X. He, Z. Niu, H. Xue, W. Jiang, L. Ying, W. Peng, M. Maezawa, Z. Lin, X. Xie, *et al.*, Quasiparticle dynamics in superconducting quantum-classical hybrid circuits, *Phys. Rev. B* **108**, 064512 (2023).
- [54] D. V. Averin, K. Rabenstein, and V. K. Semenov, Rapid ballistic readout for flux qubits, *Phys. Rev. B* **73**, 094504 (2006).
- [55] A. Fedorov, A. Shnirman, G. Schön, and A. Kidiyarova-Shevchenko, Reading out the state of a flux qubit by josephson transmission line solitons, *Phys. Rev. B* **75**, 224504 (2007).
- [56] A. Herr, A. Fedorov, A. Shnirman, E. Il'ichev, and G. Schön, Design of a ballistic fluxon qubit readout, *Supercond. Sci. Technol.* **20**, S450 (2007).
- [57] O. Naaman, J. I. Park, and A. A. Pesetski, Qubit readout via resonant scattering of josephson solitons (2013), uS Patent 8,508,280.
- [58] I. I. Soloviev, N. V. Klenov, A. L. Pankratov, L. S. Revin, E. Il'ichev, and L. S. Kuzmin, Soliton scattering as a measurement tool for weak signals, *Phys. Rev. B* **92**, 014516 (2015).
- [59] W. Wustmann and K. Osborn, Rapid qubit readout dependent on the transmission of a single fluxon, *Phys. Rev. Applied* **25**, 034027 (2026).
- [60] S. Nakamura, H. Numabe, A. Bozbey, and A. Fujimaki, Current resolution of a single-flux-quantum readout circuit based on current-to-time conversion toward a flux qubit system, *IEEE Trans. Appl. Supercond.* **19**, 973 (2009).
- [61] K. G. Fedorov, A. V. Shcherbakova, M. J. Wolf, D. Beckmann, and A. V. Ustinov, Fluxon readout of a superconducting qubit, *Phys. Rev. Lett.* **112**, 160502 (2014).
- [62] S. Van Winckel, A. Caglar, B. Gys, S. Brebels, A. Potocnik, B. Parvais, P. Wambacq, and J. Craninckx, A 28nm 6.5-8.1 GHz 1.16 mW/qubit cryo-CMOS system-on-chip for superconducting qubit readout, in *ESSCIRC 2022-IEEE 48th European Solid State Circuits Conference (ESSCIRC)* (IEEE, 2022) pp. 61–64.
- [63] M. Ahmad, C. Giagkoulovits, S. Danilin, M. Weides, and H. Heidari, Scalable cryoelectronics for superconducting qubit control and readout, *Adv. Intell. Syst.* **4**, 2200079 (2022).
- [64] S. Das, S. Raman, and J. C. Bardin, A 4-to-6-GHz cryogenic CMOS LNA with 4.4-K average noise temperature in 22-nm FDSOI, *IEEE Microw. Wirel. Technol. Lett.* **34**, 411 (2024).
- [65] L. Lei, H. Huang, P. Chen, and M. Deng, Cryogenic control and readout integrated circuits for solid-state quantum computing, arXiv:2410.15895 (2024).
- [66] J. Keener and D. McLaughlin, Solitons under perturbations, *Phys. Rev. A* **16**, 777 (1977).
- [67] D. W. McLaughlin and A. C. Scott, Perturbation analysis of fluxon dynamics, *Phys. Rev. A* **18**, 1652 (1978).
- [68] L. Aslamazov and E. Gurovich, Pinning of solitons by abrikosov vortices in distributed josephson junctions, *JETP Lett.* **40** (1984).
- [69] M. M. Wildermuth, *Quantum tunneling of Josephson vortices in high-impedance long junctions* (KIT Scientific Publishing, 2023).
- [70] T. Kato and M. Imada, Macroscopic quantum tunneling of a fluxon in a long josephson junction, *J. Phys. Soc. Jpn.* **65**, 2963 (1996).
- [71] A. Kemp, A. Wallraff, and A. V. Ustinov, Josephson vortex qubit: Design, preparation and read-out, *Phys. Status Solidi (b)* **233**, 472 (2002).

- [72] M. Wildermuth, L. Powalla, J. N. Voss, Y. Schön, A. Schneider, M. V. Fistul, H. Rotzinger, and A. V. Ustinov, Fluxons in high-impedance long josephson junctions, *Appl. Phys. Lett.* **120**, 112601 (2022).
- [73] A. Matsuda and S. Uehara, Observation of fluxon propagation on josephson transmission line, *Appl. Phys. Lett.* **41**, 770 (1982).
- [74] A. Matsuda and T. Kawakami, Fluxon propagation on a josephson transmission line, *Phys. Rev. Lett.* **51**, 694 (1983).
- [75] M. Gubrud, M. Ejrnaes, A. Berkley, R. Ramos, I. Jin, J. Anderson, A. Dragt, C. Lobb, and F. Wellstood, Sub-gap leakage in Nb/AlO<sub>x</sub>/Nb and Al/AlO<sub>x</sub>/sub x//Al josephson junctions, *IEEE Trans. Appl. Supercond.* **11**, 1002 (2002).
- [76] A. Ustinov, T. Doderer, R. Huebener, N. Pedersen, B. Mayer, and V. Oboznov, Dynamics of sine-gordon solitons in the annular josephson junction, *Phys. Rev. Lett.* **69**, 1815 (1992).
- [77] D. T. Le, A. Fedorov, and T. M. Stace, Microwave circulation in an extended josephson junction ring, *Phys. Rev. Lett.* **135**, 230801 (2025).
- [78] S. B. Kaplan, A. F. Kirichenko, O. A. Mukhanov, and S. Sarwana, A prescaler circuit for a superconductive time-to-digital converter, *IEEE Trans. Appl. Supercond.* **11**, 513 (2001).
- [79] Q. P. Herr, M. W. Johnson, and M. J. Feldman, Temperature-dependent bit-error rate of a clocked superconducting digital circuit, *IEEE Trans. Appl. Supercond.* **9**, 3594 (2002).
- [80] G. S. Lee, R. C. Ruby, H. L. Ko, and A. T. Barfknecht, Superconducting race arbiter with subpicosecond timing discrimination, *Appl. Phys. Lett.* **59**, 2892 (1991).
- [81] A. Kirichenko, S. Sarwana, D. Gupta, I. Rochwarger, and O. Mukhanov, Multi-channel time digitizing systems, *IEEE Trans. Appl. Supercond.* **13**, 454 (2003).
- [82] H. Terai, Z. Wang, Y. Hishimoto, S. Yorozu, A. Fujimaki, and N. Yoshikawa, Timing jitter measurement of single-flux-quantum pulse in josephson transmission line, *Appl. Phys. Lett.* **84**, 2133 (2004).
- [83] K. Nakamiya, T. Nishigai, N. Yoshikawa, A. Fujimaki, H. Terai, and S. Yorozu, Improvement of time resolution of the double-oscillator time-to-digital converter using sfq circuits, *Physica C* **463**, 1088 (2007).
- [84] M. Terabe, A. Sekiya, T. Yamada, and A. Fujimaki, Timing jitter measurement in single-flux-quantum circuits based on time-to-digital converters with high time-resolution, *IEEE Trans. Appl. Supercond.* **17**, 552 (2007).
- [85] E. Kim, X. Zhang, V. S. Ferreira, J. Banker, J. K. Iverson, A. Sipahigil, M. Bello, A. González-Tudela, M. Mirhosseini, and O. Painter, Quantum electrodynamics in a topological waveguide, *Phys. Rev. X* **11**, 0111015 (2021).
- [86] V. Jouanny, S. Frasca, V. J. Weibel, L. Peyruchat, M. Scigliuzzo, F. Oppliger, F. De Palma, D. Sbroggiò, G. Beaulieu, O. Zilberberg, *et al.*, High kinetic inductance cavity arrays for compact band engineering and topology-based disorder meters, *Nat. Commun.* **16**, 3396 (2025).
- [87] A. Glezer Moshe, E. Farber, and G. Deutscher, Granular superconductors for high kinetic inductance and low loss quantum devices, *Appl. Phys. Lett.* **117** (2020).
- [88] D. López-Núñez, A. Torras-Coloma, Q. Portell-Montserrat, E. Bertoldo, L. Cozzolino, G. A. Um-marino, A. Zaccone, G. Rius, M. Martinez, and P. Forn-Díaz, Superconducting penetration depth of aluminum thin films, *Supercond. Sci. Technol.* **38**, 095004 (2025).
- [89] S. Coleman, Quantum sine-gordon equation as the massive thirring model, *Phys. Rev. D* **11**, 2088 (1975).
- [90] D. Esteve, M. H. Devoret, and J. M. Martinis, Effect of an arbitrary dissipative circuit on the quantum energy levels and tunneling of a josephson junction, *Phys. Rev. B* **34**, 158 (1986).
- [91] M. Neeley, M. Ansmann, R. C. Bialczak, M. Hofheinz, N. Katz, E. Lucero, A. O'Connell, H. Wang, A. Cleland, and J. M. Martinis, Transformed dissipation in superconducting quantum circuits, *Phys. Rev. B* **77**, 180508 (2008).